Towards a Structural Model for the Aluminium Tellurite Glass System

Emma Barney[1]*, Nattapol Laorodphan[2†], Faizani Mohd-Noor[2‡], Diane Holland[2], Tom Kemp[2], Dinu Iuga[2] and Ray Dupree[2]*.

[1] *Faculty of Engineering, University of Nottingham, Nottingham, NG7 2RD, UK*
[2] *Physics Department, University of Warwick, Coventry, CV4 7AL, UK*
†now at Faculty of Science, Maejo University, Chiang Mai, Thailand
‡now at Physics Dept., UTM, Johor Bahru, Malaysia

Corresponding authors: *Emma.Barney@nottingham.ac.uk; *Ray.Dupree@warwick.ac.uk

Abstract

Neutron diffraction, ^{27}Al MAS NMR and ^{27}Al Double Quantum MAS NMR results are presented and analysed to determine the local environments of the cations in a series of aluminium tellurite glasses. Total scattering results show that, within a maximum Te-O distance of 2.36 Å, tellurium exhibits a mix of [TeO_3E] and [TeO_4E] environments (E = electron lone-pair), with a linear reduction in the average tellurium-oxygen coordination number as Al_2O_3 is added to the glass. This is accompanied by a linear decrease in the average aluminium-oxygen coordination number as [AlO_4] units form at the expense of [AlO_6] units, whilst the fraction of [AlO_5] units remains roughly constant. A consideration of the bonding requirements of the five structural units in the glass, [TeO_3E], [TeO_4E], [AlO_4], [AlO_5] and [AlO_6] has allowed a direct quantitative relationship between tellurium-oxygen and aluminium-oxygen coordination numbers to be derived for the first time, and this has been successfully extended to the boron tellurite system. Double Quantum ^{27}Al MAS NMR indicates that, in contrast to previous reports, the shortest Al…Al separations are significantly smaller (~3.2 Å) than expected for a uniform distribution and there is a preference for [AlO_6]-[AlO_6] and [AlO_4]-[AlO_4] corner sharing polyhedra. These associations support a new structural model which successfully applies the principle of charge balance to describe the interaction of tellurium and aluminium and identifies and explains the clustering of [AlO_n] polyhedra in the glass and their preferred associations. [AlO_6] and [TeO_4E] units dominate the network in TeO_2-rich glasses and $[AlO_4]^-$ units form to stabilise the $[TeO_3E]^+$ units as alumina is added to the glass.

1 Introduction

Tellurite glasses have a range of superior functional properties, when compared to silica, which make them promising candidates for a range of optical applications in the near and mid infra-red (IR). These properties include: higher refractive indices,[1] larger third-order non-linear optical coefficients,[2] lower phonon energies and extended transmittance into the infra-red.[1] In addition, tellurites can solubilise larger quantities of rare-earth (RE) ions than silicates without fluorescence quenching,[3] have good ionic conductivity and exhibit high dielectric constants.[1, 4-6] However, the exploitation of tellurite glasses is often limited by low melting points, poor durability and small regions of thermal stability. To address these problems, optimised glass compositions often include a number of modifiers to control functional properties, including transition metal oxides, to increase softening temperature, and alkali oxides, to improve glass stability. How these modifiers interact with the glass network, and each other, to give rise to the property changes is still poorly understood.

Full exploitation of the potential of tellurite glasses requires an understanding of the interdependence of glass composition, structure, and functional properties. A number of studies have shown that the tellurium environment is converted from four-coordinated pseudo-trigonal bipyramid structures ($[TeO_4E]$) in TeO_2-rich glasses, to pseudo-tetrahedral $[TeO_3E]$ units (E represents the electron lone-pair and is henceforth omitted) as modifier (X_nO_m) is added to the glass network.[7-10] In these discussions there was an underpinning assumption that the tellurium-oxygen coordination number for a glass of a particular composition will match that of an analogous tellurite crystal (i.e. amorphous TeO_2, like α-TeO_2, will be entirely composed of $[TeO_4]$ units) and the change in coordination number is driven by the need to accommodate the modifier in the network.[11-12] These two assumptions suggest that there should be a smooth and linear change in tellurium-oxygen coordination number, n_{TeO}, with modifier content. Our recent measurement of amorphous TeO_2 has yielded a tellurium-oxygen coordination number of 3.68(4)[13] which necessitates that ~1/3 of tellurium atoms in amorphous TeO_2 are in $[TeO_3]$ environments and, to preserve stoichiometry, ~1/6 of oxygen atoms must form terminal Te=O bonds.[13-14] This result has been critical to developing a model that accurately predicts the non-linear variation in tellurium-oxygen coordination number with composition in potassium tellurite glasses,[13] and subsequent work demonstrated that the model is applicable to other alkali-modified glasses.[14] Changes in tellurium-oxygen coordination number were used to explain changes in functional properties with composition, including: glass transition temperature, T_g,[14] the change in the activation energy of enthalpy relaxation,[15-17] the mean square displacement of Te as measured by Mossbauer in sodium tellurite glasses,[15-17] the AC conductivity of tellurite glasses,[18-20] and the conductivity of lithium tellurite glasses.[21] It is important

to extend this insight to achieve a better understanding of the roles that non-alkali oxides play in modifying the network structure of tellurite glasses.

The addition of alumina to a tellurite glass can strongly alter its functional properties with small amounts of Al_2O_3 having significant effects on thermal properties such as T_g and glass stability, ΔT (= $T_x - T_g$ where T_x is the onset of the first devitrification event). The addition of 2.5 mol% Al_2O_3, for instance, to a silver tellurite glass was shown to increase glass stability by 32 °C [22] and the substitution of 2 mol% Al_2O_3 in place of ZnO in an Yb_2O_3 doped zinc potassium tellurite glass increased T_g by 26 °C and ΔT by 20 °C.[23] Furthermore alumina is known to improve optical properties by improving the dispersion of RE ions in glasses. Wang *et al*.[23] demonstrated that 2 mol% Al_2O_3 in a Yb_2O_3 doped tellurite glass increased emission cross section by 0.5 pm^2 and increased fluorescence lifetime by 0.19 ms and Nogami and Abe [24] showed that the substitution of 10 mol% Al_2O_3 into a silicate glass doped with 5 wt% Eu_2O_3 increased fluorescence by a factor of 2. They attributed this improvement in fluorescence to the preferential association of the RE^{3+} ion with Al-O^- bonds in [AlO_6] polyhedra resulting in better dispersion of RE ions through the glass.[24] Understanding the role of Al_2O_3 in tellurite glasses is also important because a number of studies in the literature have measured the functional properties of tellurite glasses melted in alumina crucibles. It has been shown that between 2.5 [22] and 18 [25] mol% Al_2O_3 can enter a tellurite glass network when melted in alumina crucibles and this has an important effect on the structure and properties of the glass. For example, a study of Ag_2O-TeO_2 glasses showed that when melting in alumina the concentration of Al_2O_3, homogeneity, colour and thermal properties of the glass obtained varied with melting time.[22]

The strong variation in the functional properties, including increased glass stability and increased fluorescence, that alumina can impart to a tellurite glass allows us to infer that Al_2O_3 plays a significant role in modifying the network structure. However, there have been very few studies to investigate the interaction of aluminium and tellurium in a glass network. One XANES and EXAFS study of aluminium tellurites has shown that the tellurium environments in the glass become increasingly three-coordinated as Al_2O_3 is added to the network.[2] Raman spectra for tellurites modified with 1, 2, 3 and 4 mol% Al_2O_3 showed a rapid increase in the intensity of the peak at 740 cm^{-1} [26] which was attributed to vibrations of [TeO_3] units, indicating their formation even at low modifier concentrations. A ^{27}Al and ^{125}Te NMR study of the Al_2O_3-TeO_2 binary glasses containing up to 14.3 mol% Al_2O_3 showed that aluminium adopts a mix of 4, 5 and 6 coordinated sites and the fractions of the higher coordinated species of both [AlO_n] and [TeO_n] decrease with added modifier[27] whilst a ^{27}Al MAS NMR study of Al_2O_3-Ta_2O_5-TeO_2 glasses also demonstrated that the average

aluminium coordination number decreases as Al_2O_3 replaces TeO_2 in the glass.[28] Recently Kaur *et al*.[29] presented a combination of Raman spectroscopy and ^{27}Al MAS NMR to qualitatively show that, in glasses containing between 1 and 20 mol% Al_2O_3, both the tellurium and aluminium coordination number decrease as aluminium is added to the glass. The present study is the first to combine neutron diffraction and advanced ^{27}Al MAS NMR to provide a quantitative measurement of the local environments of *both* aluminium and tellurium in a series of aluminium tellurite glasses. It successfully applies the principle of charge balance to derive a new structural model to describe their interaction and furthermore identifies and explains the clustering of [AlO_n] polyhedra that is observed in the glass and their preferred associations.

2 Experimental section

2.1 Sample preparation and characterisation

Aluminium tellurite glasses with nominal compositions of 5, 10, 15 and 20 mol% Al_2O_3 were prepared by placing a suitable mixture of Al_2O_3 (Alfa Aesar, > 99 mol%) and TeO_2 (Alfa Aesar, 99.99 mol%) in Pt/Rh crucibles and heating to 800 °C, at a ramp rate of 5 °C/minute. All glasses were modified with 0.1 mol% Fe_2O_3 to shorten data collection times in NMR experiments. The glass melt was held at temperature for 30 minutes before being splat-quenched using steel plates. Where appropriate, results for these glasses are compared with those obtained for a bulk sample of pure amorphous TeO_2, the preparation of which has been reported previously.[13]

The precursor chemicals were carefully weighed and mixed before melting to ensure that the resultant glass would be as homogeneous as possible. However, when quenching the glasses, a macroscopic phase separation was observed for the nominally 15 and 20 mol% Al_2O_3 aluminium tellurite glasses, with the formation of clear and cloudy areas of sample. X-ray diffraction was used to identify the components of the cloudy regions but, otherwise, only the clear portions of the glass were selected for further experiments. The compositions of all clear samples were measured using a PANalytical MiniPal4 to collect X-ray Fluorescence (XRF) spectra. Following initial analysis, an additional aluminium tellurite glass containing 2.5 mol% Al_2O_3 was produced for the neutron diffraction and NMR experiments.

Density measurements were carried out on the clear samples using a Micromeritics pycnometer with helium as the displacement fluid and the values compared with the literature. For the 15 and 20 mol% Al_2O_3 aluminium tellurite samples there was significant discrepancy between measured and literature densities indicating that the compositions for these samples differ from the nominal. Two methods were used to determine an accurate composition for each sample. Firstly, XRF analysis was

performed, as above, and Table 1 gives the concentration of Al_2O_3 after scaling relative to that measured for the 5 mol% Al_2O_3 sample. The second approach was to calculate the composition of each sample by comparing its measured density to the line of best fit through the literature data shown in Figure S1. The results from this analysis are also given in Table 1 and there is excellent agreement between the compositions determined by XRF and density measurements. The revised glass compositions used in all future analysis are x = 2.5, 5, 10, 12.5 and 16 mol% Al_2O_3.

Differential thermal analysis (DTA) was performed using a DTA 673-4 1500C thermal analyser with alumina as reference and Pt/10Rh crucibles. The sample and reference were heated at 10 °C/minute to 600 °C – 800 °C (depending on alumina content) and then allowed to Newtonian cool.

Scanning electron microscopy (Zeiss SUPRA 55-VP 20 kV) and micro-Raman spectroscopy (Horiba LabRam Evo Spectrometer, 488 nm, x50 objective) were performed on the 10 and 12.5 % Al_2O_3 samples in order to obtain further information on the microstructure in these samples.

2.2 Neutron diffraction

The glass fragments were placed inside a cylindrical vanadium container of inner diameter 8.3 mm for the neutron diffraction measurements. These containers were thin-walled, with a vanadium thickness of 25 µm, in order to reduce the magnitude of the experimental corrections. The neutron diffraction patterns were measured using the GeM diffractometer [30] at the ISIS neutron spallation source (Rutherford Appleton Laboratory, Oxfordshire, UK). Measurements of an 8 mm diameter vanadium rod, the empty instrument and empty container were made for normalisation and data corrections. The scattering data were reduced and corrected for attenuation, multiple scattering and self scattering using standard Gudrun [31] and ATLAS [32] software to give the distinct scattering, $i(Q)$. These $i(Q)$ v Q spectra were fitted with a quadratic, of the form A+BQ^2, at low Q to extrapolate the data to Q = 0. Once fully corrected, the $i(Q)$ data were Fourier transformed, with a maximum momentum transfer, Q_{max}, of 35 Å^{-1}. This yielded the total correlation functions, $T(r)$, of the form:

$$T(r) = 4\pi\rho^0 r + \frac{2}{\pi}\int_0^{Q_{\max}} Qi(Q)M(Q)\sin(rQ)\,dQ \qquad (1)$$

where ρ^0 is the atomic number density and $M(Q)$ is the Lorch modification function used to reduce the termination ripples in $T(r)$ that arise from the finite maximum experimental value of Q.[33] The resolution in real-space depends upon the modification function used and the maximum momentum transfer, $Q_{\max}$, of the experimental data. Each correlation function is a weighted summation over all the pairwise combinations of elements in the sample, $t_{ll'}(r)$:

$$T(r) = \sum_{l,l'} c_l b_l \, b_{l'} t_{ll'}(r) \quad (2)$$

where c_l is the atomic fraction and b_l is the coherent neutron scattering length of element l. Any resolvable peak in $T(r)$ that arises solely from interatomic distances between atoms of element l and l' can be fitted to extract an area, $A_{ll'}$, and position, $r_{ll'}$, for the peak. Using these parameters, along with the weighted coefficient for $t_{ll'}(r)$ given in Equation 2, the coordination number, $n_{ll'}$, can be calculated according to

$$n_{ll'} = \frac{r_{ll'} A_{ll'}}{(2 - \delta_{ll'}) c_l b_l b_{l'}} \quad (3)$$

where $\delta_{ll'}$ is the Kronecker delta.

Calculations of the contribution of the Al-O peak to $T(r)$, subtraction of the Al-O peak and subsequent fitting to the residual Te-O peak were carried out using the ATLAS software.[32]

2.3 ^{27}Al MAS-NMR

Most ^{27}Al MAS NMR spectra were taken at 221.5 MHz using a Bruker Avance III 850 MHz (20 T) spectrometer with a 3.2 mm probe spinning at an MAS frequency of 20 kHz. For the 1D experiments, a pulse width of 0.8 μs (π/6) was used. The spectra were referenced to the [AlO_6] peak in yttrium aluminium garnet (YAG), which was set at 0.7 ppm with respect to the primary reference 0.1M aqueous $[Al(H_2O)_6]^{3+}$. 1D spectra were also taken at 11.75 T using a Bruker Avance III 500 MHz spectrometer and at 14.1 T using a Bruker Avance II+ 600 MHz spectrometer. In both cases, 3.2 mm probes were used with MAS frequency 15 kHz. At 11.75 T a pulse width of 0.5 μs was used whilst, at 14.1 T, the pulse width was 1.35 μs; a recycle delay of 5s was used for the majority of 1D experiments. The spectra for glasses with 12.5 and 16 mol% alumina content showed evidence of a small amount of crystallisation, affecting the [AlO_6] peak. However, the crystalline material had a much longer relaxation time, T_1, (see figure S2) so that use of a shortened recycle delay of 0.25 s for the 12.5 mol% Al_2O_3 sample spectrum ensured that the crystal phase made an almost negligible contribution to the signal and allowed 2D experiments to be performed in a reasonable time. Double quantum (DQ) experiments were performed on this sample using a $R2_2^1$ symmetry-based sequence for DQ homonuclear recoupling with a recoupling radio-frequency that matches a rotary resonance condition (n=2)[34] i.e. with an effective rf field strength of 40kHz (13.33 kHz solution value). For this sequence, sensitivity is dependent on the offset frequency used and both the power level for the recoupling pulses and the offset were optimised experimentally choosing a frequency near the [AlO_5] resonance. Spectra were taken at five different mixing times from 0.8 ms to 3.2 ms and the integrated intensities of the features in the DQ spectra were used to construct build-up

curves. For each mixing time, between 144 and 256 t_1 slices were acquired with 512 co-added transients and a recycle delay of 0.25 s. The States procedure[35] was applied to obtain phase sensitive spectra.

2.4 Simulation of ^{27}Al NMR Double Quantum build-up curves

The simulations to determine the build-up of the DQ signal for various dipolar couplings, and thus the internuclear distances, were conducted using SIMPSON[36] to determine how the signal increases as the mixing time becomes longer. The simulations replicated the experiment as described by Wang *et al*.[37] The parameters (shift, δ_{iso}; quadrupole coupling constant, $C_{Q;}$ and asymmetry parameter, η) for the different sites were selected to be consistent with the 1D ^{27}Al NMR spectra. The build-up curves and the DQ efficiency were found to be only weakly dependent on C_Q and η. The number of gamma angles was set to 7 and the crystal file was selected to be REP 66, chosen to be large enough that the results were reliable but so that computational power did not become a problem. The dipole vector and the major axis of the electric field gradient were parallel. Although the calculated maximum signal intensity changed when the axes were made perpendicular the signal build-up curve was similar. The intensity of the signal was determined by taking the first point of the FID.

2.5 ^{125}Te NMR

Static ^{125}Te NMR was performed at 4.7 T using a 7.5 mm Varian probe tuned to a frequency of 63.2 MHz. Spectra were obtained using a τ - t - 2τ pulse echo sequence with τ = 2 μs (~π/2) and a sweep width of 500 kHz. A 30 s pulse delay was sufficient to give quantitative spectra. Spectra were accumulated with typically 10000 acquisitions and 2 - 4 kHz line broadening was applied to suppress noise. A 1M aqueous solution of telluric acid was used as the chemical shift reference (713 ppm with respect to the primary reference $(CH_3)_2Te$).

3 Results

3.1 Sample characterisation

The thermal analysis scans of the clear samples in Figure 1a show that there is a single glass transition temperature, T_g, for amorphous TeO_2. However, for all of the aluminium tellurite samples, two T_g events are observed. The measured T_g values are given in Table 1 and are plotted in Figure 1b to show that both T_g values increase linearly with alumina content, when the revised compositions are used. This is further evidence that the correct compositions have been determined. Two T_g events were also reported by Kaur *et al*. for a 20 mol% Al_2O_3 sample but the rest of their samples contained only 7 mol% or less Al_2O_3 and no second T_g was visible.[29]

3.2 Neutron diffraction

Figure 2 shows the distinct scattering data, $i(Q)$, measured for the aluminium tellurite glasses. The data measured for samples containing between 2.5 and 10 mol% Al_2O_3 exhibit no Bragg peaks, indicating that samples of these compositions are fully amorphous. Despite the use of only clear portions of sample, the glass modified with 12.5 mol% Al_2O_3 has some slight evidence of crystallinity in $i(Q)$ while that modified with 16 mol% Al_2O_3 additionally exhibits sharp, well-defined Bragg peaks from α-Al_2O_3 in addition to the main glass features. Figure S3 in supplementary information shows the low Q region of $i(Q)$ in more detail for the samples exhibiting Bragg peaks.

The total correlation functions, $T(r)$, for each aluminium tellurite sample are shown in Figure 3 with the previously reported correlation function for amorphous TeO_2.[13] The correlation functions for the aluminium-tellurite samples show a marked similarity to amorphous TeO_2, exhibiting two peaks centred at ~1.9 Å and ~2.8 Å. The first peak in amorphous TeO_2 has a broad distribution and has been attributed to Te-O bond lengths present in the glass, while the second peak is attributed predominately to O-O distances. The lack of a separate peak in the aluminium tellurites arising from Al-O bond lengths indicates that there is a significant overlap of the Te-O and Al-O distances in these glasses. It is necessary to deconvolute these two contributions to the first peak in the correlation function before the tellurium-oxygen coordination number, n_{TeO}, can be measured.

3.3 ^{27}Al MAS NMR

3.3.1 1-D MAS NMR

Figure 4 shows the ^{27}Al MAS NMR spectra for each sample measured at 20 T. All samples have three broad peaks centred at approximately 6, 32 and 56 ppm which arise from [AlO_6], [AlO_5] and [AlO_4] environments in the glass respectively. They are sufficiently well resolved at this field to allow accurate deconvolution of the data. The assignment is based on observations of Al^{3+} in glasses and minerals[38-41] and the shifts are consistent with those reported by Kaur *et al*.[29] and Sakida *et al*.[27] for the Al_2O_3-TeO_2 system. Although the 12.5 and 16 mol% Al_2O_3 glasses give predominantly broad amorphous NMR spectra, they have a small sharp feature (hardly noticeable for the 12.5 % sample) at ~6 ppm that overlaps with the [AlO_6] peak from the amorphous phase. In addition, the 16 mol% Al_2O_3 spectrum has a second, stronger, sharp peak at ~15 ppm. The samples have been doped with 0.1 mol% Fe_2O_3 with the Fe ions dispersed throughout the glass network. However, the Fe ions do not appear to be substituted in the crystal phases since the aluminium nuclei in the glass have a significantly (>> 10 times) faster relaxation rate than those in the crystal phases. Figure S2 in the supplementary information shows a series of spectra collected for the 16 mol% sample with different delays. The shapes and relative intensities of the [AlO_4] and [AlO_5] peaks are unchanged as

the recycle delay is reduced. Similarly, for the 12.5 mol. % sample, where there is only a small amount of crystalline material, the relative intensity of the [AlO_6] glass peak is unchanged down to the shortest recycle delay used, 0.05s, allowing accurate measurement of the relative amounts of the three co-ordination environments in the glass.

The proportions of aluminium in the three environments in the glasses were determined using 4 s pulse delay spectra for the four lowest Al_2O_3 concentrations and, to ensure minimal contribution from the crystalline phase, a 0.05 s pulse delay spectrum for the highest Al_2O_3 content sample. The contributions from the [AlO_4] and [AlO_5] species to the centre band peaks were approximated as Gaussian line shapes and that from the [AlO_6] as either a pseudo-Voigt (70% Lorentzian) line shape or a biGaussian line shape – the latter being the procedure adopted by Sakida *et al*.,[27] both giving similar results. As a further check the centre band peaks were also integrated to find the peak areas using a region of interest for each peak defined by the minima separating it from its neighbouring peaks. The three approaches gave values which agree within error ($\pm$ 1%) for all but the 16 mol% Al_2O_3 sample, where the crystal peaks proved to be incompletely suppressed even by the 0.05 s pulse delay (see Figure S2 for effect of changing pulse delay). The percentages of [AlO_4], [AlO_5] and [AlO_6] units are given in Table 2 and are also shown in Figure 5 where the values can be compared with those reported by Sakida *et al*.[27] and Kaur *et al*.[29]

^{27}Al NMR spectra were also collected at two additional fields, 11.75 and 14.1 T, in order to estimate the chemical shift dispersion and quadrupole parameters for each [AlO_n] species. Figure S4a in supplementary information shows the NMR spectra collected at the three fields for the 10 mol% Al_2O_3 aluminium tellurite sample, chosen for the absence of crystal peaks. A comparison of the NMR spectra shows a progressive narrowing of the peaks with increasing field and a gradual downfield shift of the peak centre of gravity, δ_{cog}, which is related to the isotropic chemical shift for ^{27}Al, nuclear spin I = 5/2, by

$$\delta_{cog} = \delta_{iso} - \frac{3}{500}\frac{P_Q^2}{\nu_0^2} \qquad (4)$$

where ν_0 is the Larmor frequency of ^{27}Al at the given field; and P_Q is the quadrupole coupling product.

$$P_Q^2 = C_Q^2(1 + \eta^2/3) \qquad (5)$$

C_Q is the mean nuclear quadrupole coupling constant (which is a measure of the electric field gradient (EFG) around the nucleus) and η, where $0 \leq \eta \leq 1$, the asymmetry parameter.[38] Figure S4b

shows a plot of δ_{cog} versus $1/(\nu_0)^2$ for the various [AlO_n] species at the different fields. Fitting straight lines to the plots gives an intercept of δ_{iso} and a slope of $-3P_Q^2/500$ from which values of C_Q can be extracted if an estimate of η is available. The values of the parameters obtained using equations 4 and 5 are summarised in Table 3.

Chemical shift dispersion (csd) is an important parameter for glasses since it reflects the distributions in the structural parameters which describe the range of environments experienced by a nucleus in an amorphous material. Since the MAS peak width contains contributions from both the 2nd order quadrupolar interaction (inversely proportional to field) and from csd (proportional to field) information about the csd associated with each site can be obtained from the change in peak width with field. For Gaussian lines, such as are observed here, if measurements are taken at two fields B_1 and B_2 the full-widths at half-maximum can be expressed as [42]

$$FWHM_1^2 = W_Q^2 + W_{csd}^2$$
$$FWHM_2^2 = \left(\frac{B_1}{B_2}\right)^2 W_Q^2 + \left(\frac{B_2}{B_1}\right)^2 W_{csd}^2 \qquad (6)$$

where W_{csd} is the contribution from the chemical shift dispersion and W_Q the contribution from quadrupolar broadening. The values obtained for W_Q and W_{csd} for [AlO_4], [AlO_5] and [AlO_6] in the 10 mol% Al_2O_3 glass are summarised in Table 3 which shows that the chemical shift dispersion is the major contribution to the linewidth for all of the sites at this 20T.

3.3.2 Double quantum (DQ) homonuclear NMR

A DQ MAS NMR experiment is a powerful method for probing the spatial distribution of aluminium nuclei because the DQ signal is strongly dependent on the distance *r* between atoms, since the dipolar coupling constant, b_{ij} (in Hz), between nuclei i and j is

$$b_{ij} = \mu_0 \frac{-\gamma^2 \hbar}{8\pi^2 r_{ij}^3} \qquad (7)$$

Note that, as we are dealing with a glass, there will be a range of distances and of relative orientations of the dipolar vector and electric field gradient which will affect both the DQ efficiency and the signal build-up. Nevertheless, if the aluminium nuclei were distributed uniformly throughout the glass, the dipolar coupling would be so weak (~30 Hz) that the DQ signal would be almost unobservable.[43] In the 2D DQ spectrum, peaks that arise along the diagonal line, (ω, 2ω), are autocorrelation peaks which indicates a dipolar interaction between two atoms with the same chemical shift. Off-diagonal pairs of interactions, (ω_A, ω_A+ ω_B) and (ω_B, ω_A+ ω_B), correspond to correlations between atoms with different chemical shifts. Figure 6 shows the DQ spectrum

measured for the 12.5 mol% Al_2O_3 aluminium tellurite glass using a mixing time of 3.2 ms. The two strongest peaks are the autocorrelation peaks at (6, 12) and (54, 108), which correspond to interactions between two [AlO_6] units and two [AlO_4] units respectively. This indicates that there is strong clustering of like pairs of [AlO_6] and [AlO_4] but not [AlO_5]. The signals measured for the off-diagonal pairs are weaker, indicating longer distances between unlike aluminium units. There is a weak peak at (33, 66) seen more clearly in slices taken through the spectrum near this point on the DQ axis (Figure S5 in SI), which arise from the interaction between two [AlO_5] units indicating that these units are significantly further apart than other autocorrelation pairs, suggesting a more random distribution of this species.

Figure 7 shows the experimentally measured build-up curve for interactions between two [AlO_6] units, taken from measurements at five different mixing times, together with simulated curves calculated using SIMPSON.[36] The simulations used the C_Q values given in Table 3 for the 12.5 mol% Al_2O_3 sample and η was assumed to be 0.5. Each simulated line is for a dipolar coupling frequency corresponding to a 5% change in the distance between a pair of atoms. Note that these simulations are for isolated pairs of nuclei and for longer mixing times the effect of more distant aluminium nuclei will become important, thus the magnitude of the dipolar coupling is most easily determined from the initial part of the build-up. Furthermore, since our samples are glasses with a range of distances, it is the shortest distance, with the strongest dipolar coupling, which will give the fastest and strongest build-up. The initial build-up for the [AlO_6]-[AlO_6] correlation in Figure 7 corresponds most closely to a dipolar coupling of ~250 Hz, a distance of ~3.2 Å. The build-up curves for all six [AlO_n]-[AlO_m] configurations are shown in Figure S6 in the supplementary information. The distances associated with the build-up curves that most closely match each interaction are given in Table 4.

4 Discussion

4.1 Sample Characterisation

4.1.1 Phase formation

The synthesis conditions for the glasses used in this study (see Section 2.1) were almost identical to those used by Kaur (heat to 850 °C; 30 min hold; splat quench), Tagiara (heat to 800 - 900 °C; 30 min hold; splat quench between pre-heated plates) and Sakida (heat to 820-950°C; 10 min hold; splat quench). The nominally 15 and 20 mol.% Al_2O_3 aluminium tellurite glasses exhibited large scale phase separation into clear and cloudy portions. Similar separation has been observed in the boron tellurite glass system (> 20 mol% B_2O_3) which may provide a model for the immiscibility in the aluminium tellurite system.[44-46] The cloudy glass pieces were not part of the structural study,

however the XRD pattern from those portions of the nominal 20 mol% Al_2O_3 cloudy showed diffraction peaks from α-Al_2O_3 and also from the oxidised phase, aluminium tellurate, $Al_2Te_4O_6$[47] in addition to >90 % residual glass. The compositional analysis of the clear phases for 15 and 20 mol.% Al_2O_3, carried out using density and XRF measurements, shows that they have a higher TeO_2 content than the nominal value (Table 1). A similar effect is observed in boron tellurites. Density values (Figure S1) measured for the 5 and 10 mol.% Al_2O_3 glasses matched the values reported in the literature for these compositions. The two T_g events observed by DTA (Figure 1a) for all the *clear* aluminium tellurite glasses studied indicate the presence of a glass-in-glass phase separated structure of dimension significantly smaller than the wavelength of visible light. Micro-Raman, electron microscopy and an examination of the low Q region of the neutron diffraction data have failed to yield more information about the nature of the phase separation. The linear change with composition of both glass transition temperatures (Figure 1b) suggests that, rather than the nucleation and growth of one fixed composition phase such as amorphous TeO_2 in a second Al_2O_3-containing glass phase, there is spinodal decomposition into two glass phases of varying composition. Plotting the lower glass transition temperatures, T_{g1}, against the measured overall composition of the glasses results in a trend line which passes though the expected value of T_g for amorphous TeO_2 and the published values for single phase aluminium tellurite glasses.[26, 29] The near parallel trend of the higher glass transition temperatures, T_{g2}, measured would, if due to the same compositional dependence, indicate an ~8 mol% difference in Al_2O_3 content between the two phases, with the higher T_g arising from an Al_2O_3 rich glass. The glass phases that form can therefore be considered as one series based on the structure of TeO_2 glass, modified with increasing amounts of Al_2O_3, and a second series of glasses, possibly related to an $Al_2Te_4O_7$ crystal phase.[48] Two T_g values are reported by Kaur et al. for a 20 mol.% Al_2O_3 aluminium tellurite glass, and they fit the trends observed in this study.[29] Comparing the results from these two studies suggests that phase separation occurs in Al_2O_3-TeO_2 glasses composed of ≥ 5 mol.% Al_2O_3.

It is not possible to quantify the amount of each phase in the glass accurately. However, a qualitative assessment can be made using the observations outlined above. There is the good agreement between the measured density of the 5 and 10 mol% Al_2O_3 aluminium tellurite glasses with the literature, and this, supported by EDX analysis, indicates that the overall composition of these two glasses has not varied significantly from the nominal value. Furthermore, the close agreement between the trendline fitted through the T_{g1} values in Figure 1b with the T_g temperatures reported for single phase glasses, indicates that, for each glass, the composition of the T_{g1} phase matches the nominal glass composition. If the 5 or 10 mol% Al_2O_3 aluminium tellurite glasses were composed of a significant amount of the second, higher T_{g2}, phases then the bulk density of the glass would not

match the density of the nominal composition. For example, a glass composed of 70% of the T_{g1} phase (nominal composition) and 30% of the T_{g2} phase (the Al_2O_3 rich phase) would have a density ~0.1 gcm^{-3} lower than the density for the nominal composition. This difference, which is much larger than the error in the measurement, is not observed and so it is likely that the high alumina glass phase yielding the higher T_g values is present as significantly less than 30% of the glass.

Further comments on the microstructure of the glasses used in the current study can be found in the SI.

4.1.2 ^{27}Al 1D NMR

Table 2 and Figure 5 give a comparison of [AlO_n] species concentration in these glasses with the values reported by Sakida *et al*.[27] (data taken at 9.4 T) and Kaur *et al*.[29] (data taken at 11.74 T). Whilst there is general agreement on the trends with composition, there are some differences which are most probably due to the much poorer resolution of their lower field data owing to the significantly larger quadrupole line broadening (proportional $1/B_0$). It is clear that increasing addition of Al_2O_3 to the TeO_2 glass network causes a reduction in the fraction of [AlO_6] units and a corresponding increase in the fraction of [AlO_4] units. As a result, the average aluminium-oxygen coordination number reduced from 5.31(5) in the 2.5 mol% Al_2O_3 aluminium tellurite glass to 4.98(5) in the glass containing 16 mol% Al_2O_3. Similar trends were also seen by Youngman and Aitken in the more complex Al_2O_3-Ta_2O_5-TeO_2 glass system.[28] Table 2 also gives the peak (centroid) positions which, within error, are invariant with composition. The multifield data allow estimation of the δ_{iso}, the chemical shift dispersion, and the quadrupole product values (Table 3) with the shifts obtained by Sakida *et al*. being similar to those reported here.[27]

The occurrence of three aluminium co-ordination states in glasses is uncommon. In alkali (alkaline earth) aluminosilicate glasses ($R_2O(R'O)$-Al_2O_3-SiO_2) in the per-alkaline composition range ($R_2O(R'O)/Al_2O_3 > 1$) aluminium is usually present as [AlO_4] charge-balanced by $R^+(R'^{2+})$.[42, 49] In the less-common, per-aluminous ($R_2O(R'O)/Al_2O_3 < 1$) glasses, [AlO_5] and small amounts of [AlO_6] are also present.[49-50] However, the Al_2O_3-SiO_2 glass series, like the Al_2O_3-TeO_2 series, is composed of two network formers and in fast quenched binary Al_2O_3-SiO_2 glasses significant amounts of all three co-ordinations are observed. It is postulated that this mix of coordination states occurs because a network of [SiO_4] and [AlO_4] tetrahedra are charge balanced via the formation of 5- and 6-coordinated Al.[40, 51] Large quantities of each coordination state are also observed in sol-gel prepared samples of Al_2O_3-SiO_2 and Al_2O_3-P_2O_5 glasses.[43, 52]

The three co-ordination states are also observed in amorphous alumina prepared by various routes: anodic films;[39, 53] thin films (predominantly [AlO_4] and [AlO_5]);[43] and sol-gel (also mainly [AlO_4] and

[AlO_5]).[43, 54] However, in these cases the Al(IV) isotropic shift is significantly (> + 10 ppm) bigger and the P_Qs are much larger (~7.5 MHz for films formed from aqueous solutions)[43] than observed here for the tellurite glasses, indicating a very different local environment. Figure S7 in supplementary information compares the isotropic shifts for the various [AlO_n] species observed in amorphous Al_2O_3 and also in binary and ternary aluminate glasses. The δ_{iso} values show a linear decrease with increasing mean electronegativity (Allred-Rochow) calculated for each glass using the weighted values for the contributing cation components. The values for the Al_2O_3-TeO_2 system are consistent with this trend.

There are no reports of the ^{27}Al quadrupole parameters in Al_2O_3-TeO_2 glasses in the literature. However, the values for P_Q or C_Q (Table 3) can be compared with those for other Al-containing glasses. In Na/K aluminosilicate glasses, Schmidt *et al*.[42] obtained C_Q values for [AlO_4] of typically ~4.4 MHz for anhydrous glasses but decreasing to ~3.4 MHz in hydrous glasses, reflecting a more symmetric environment. Thomsen *et al*.[55] reported P_Q values for [AlO_4] in Na/K Ca aluminosilicate glasses ranging from 5 to 7.5 MHz depending on Al/Si ratio and charge balancing cation content. Weber *et al*.[51] found that increasing the SiO_2 content of Al_2O_3-SiO_2 binary glasses increased the P_Q values (MHz) of the different [AlO_n] species from 5.13 to 5.81 (n = 4), 5.15 to 5.5 (n = 5) and 4.22 to 4.62 (n = 6). The values reported here are similar to those found in aluminophosphate glasses (2.8 – 3.9 MHz)[52] but are generally smaller than for aluminosilicate glasses and are much smaller than for crystalline samples. This likely reflects the more symmetric environments of ^{27}Al in the tellurite network where much of the structural strain of the amorphous state can be accommodated by distortion of the [TeO_n] polyhedra, with their lone-pair of electrons, and even by coordination change. The quadrupolar coupling constant for the 10 mol% Al_2O_3 aluminium tellurite glass is largest for [AlO_4] implying that the distortion of the tetrahedron is greater than that of the [AlO_5] or [AlO_6] polyhedra.

The values obtained for W_Q and W_{csd} for [AlO_4], [AlO_5] and [AlO_6] in the 10 mol% Al_2O_3 glass are summarised in Table 3. Chemical shift dispersion is the major contribution to the line width for all three species. This reflects the large range of local environments experienced by Al, where the first coordination sphere contains 4, 5 or 6 oxygen atoms connected to either Al or Te, which in turn can have different co-ordinations: [AlO_n] (n = 4, 5, 6) or [TeO_n] (n = 3, 4). Sato *et al*.[40], investigating rapidly quenched Al_2O_3-SiO_2 glasses, measured a C_Q of approximately 3 to 3.5 MHz for both 4- and 5-coordinated Al, similar to the values found here for Al_2O_3-TeO_2 glasses. However, they reported that the width of the [AlO_4] peak was largely due to W_{csd} whilst that of [AlO_6] at 8.45T was due to W_Q.

4.2 The tellurium-oxygen coordination number

Figure 8a shows the first peak in the neutron total correlation function, $T(r)$, for 6 tellurite glasses containing between 0-16 mol% TeO_2. There is a systematic change in the area and position of the peak as increasing amounts of Al_2O_3 are added to the glass. These changes arise from the contributions of overlapping Al-O and Te-O correlations in the glass. As Al_2O_3 is added to the glass there is a shift in the peak position to shorter distances as the contribution from the Te-O peak decreases. This results in a decrease in intensity in the region of 2-2.3 Å, while the increased contribution from the Al-O peak results in an increase in intensity at ~1.75-1.9 Å

To deconvolute the two contributions to the first peak in *T(r)* it was necessary to simulate the contribution arising from the Al-O environments present in the glass. This was done using the Al speciation information obtained from the ^{27}Al MAS NMR spectra, following the process previously outlined for the tin borate glass system, where aluminium was found to be present in low concentrations.[56] To simulate a peak in *T(r)* arising from Al-O bonds it is necessary to know the position, area and width of the peak. The NMR spectra, shown in Figure 5, exhibit three peaks arising from [AlO_4], [AlO_5] and [AlO_6] environments and the relative percentages of these environments present in each glass are quantified in Table 2. From these results it is possible not only to calculate an average aluminium-oxygen coordination number, n_{AlO}, but also to calculate a likely average bond length, r_{AlO}, by using electrostatic bond strength to calculate the average Al-O bond lengths for 4-, 5- and 6- coordinated Al atoms.[57] Using these estimates for n_{AlO} and r_{AlO} it was then possible to estimate the area, A_{AlO}, of the Al-O peak in the correlation function using equation (3). Therefore, from ^{27}Al MAS NMR measurements it is possible to estimate both the average position and the area of the Al-O peak in the correlation function. Finally, a peak width of 0.1 Å^{-1} was assumed. This width is slightly broader than that used to simulate the Al-O peak in the tin borate glass system, 0.085 Å^{-1} [56] but was found, through systematic trials, to be the most appropriate thermal broadening for this system. Figure 8b shows the correlation function, $T(r)$, measured for the 16 mol% Al_2O_3 aluminium tellurite glass together with an Al-O peak simulated using the method outlined above. When the simulated peak is subtracted from the measured $T(r)$, the residual is assumed to be due solely to Te-O correlations. Figure 8c shows the extracted Te-O distribution for each composition. With the Al-O peak removed from the first peak in each $T(r)$, the residual varies linearly with composition in both size and position. As the amount of Al_2O_3 in the glass is increased, the area of the Te-O peak is reduced and the Te-O peak position shifts to shorter bond lengths. This behaviour is similar to that observed for alkali tellurites. [13-14]

The area under the Te-O peak was integrated to an r_{max} of 2.35 to calculate $\sum r_{TeO} A_{TeO}$.[58] Using these results and the partial correlation function coefficient for Te-O, $2c_{Te}\bar{b}_{Te}\bar{b}_{O}$, the total tellurium-

oxygen coordination number for each sample can be calculated using equation (3). The resultant coordination numbers are given in Table 5 and the variation with composition is plotted, along with the values for n_{AlO}, in Figure 9a. There is a correlation between the Te and Al environments, with the average coordination number of both decreasing linearly as Al_2O_3 is added to the glass. A reduction in the coordination number of tellurium is consistent with an increase in the number of [TeO_3E] units present in the glass with increased modifier content and this is in excellent agreement with the previously reported behaviour of tellurite glasses. [7-10] Furthermore, the linear changes in average coordination number for both tellurium and aluminium are consistent with the linear changes in density and T_g observed.

Figure 9b compares the rate of change of n_{TeO} for aluminium tellurites with that measured for a series of potassium tellurites[13] to show that the effect of these two modifiers on the glass network is very different. The tellurium-oxygen coordination number in potassium tellurite glasses does not vary significantly from 3.68 until more than 14.3 mol% K_2O has been added to the glass. In contrast, the tellurium-oxygen coordination number in aluminium tellurites begins to decrease immediately upon adding modifier oxide to the glass. To explain this different behaviour, a new structural model must be found. The observed relationship between the local environments of Al and Te is similar to the behaviour observed in boron tellurites,[44] where the addition of B_2O_3 to a glass results in an increase in the average boron coordination number and a decrease in the average tellurium coordination number.

4.3 A structural model for the interaction of cations in the aluminium and boron tellurite glass systems

Aluminium and boron might be expected to have a similar effect on the tellurite glass network because they both a) enter the network as M_2O_3 and b) are able to change coordination environment depending on the network structure. Therefore, this section will consider a previously proposed model for boron tellurites and how it can be adapted for the aluminium tellurite system.

Sekiya *et al.* [59-60] have previously proposed a model to explain the interaction of boron and tellurium in the boron tellurite glass system. It was suggested that the formation of [BO_4] units is concurrent with that of [TeO_3] units such that the overall positive charge on a [TeO_3] unit is compensated for by the negative charge on a [BO_4] unit. It was also proposed that these units are preferentially bonded together to provide charge balance, with every oxygen cation that is used to convert a [BO_3] unit to a [BO_4] unit necessitating the reduction of a [TeO_4] unit to a [TeO_3] unit. Based upon this model we have previously used ^{11}B MAS NMR to calculate the expected number of [TeO_3] units in the glass.[44] To make this calculation it is necessary to know the total number of Te-O bonds available in the

glass. This number can be calculated for a glass of composition x B_2O_3- $(100-x)$ TeO_2 by considering that there are there are $3x+2(100-x)$ oxygen atoms in the glass, and each of these can be assumed to form two bonds to a cation. Of these potential oxygen bonds, $2x*n_{BO}$ are required to satisfy the coordination number (n_{BO}) for the $2x$ boron atoms present in the glass. Therefore, number of oxygens with the potential to form O-Te bonds is given by $2[3x+2(100-x)]-2x*n_{BO}$ and the average number of bonds per tellurium atom is given by dividing through by the number of Te atoms in the glass, $(100-x)$:

$$n_{TeO}=\frac{2[3x+2(100-x)]-2x*n_{BO}}{100-x} \qquad (8)$$

Using equation (8) it was found that there was a large discrepancy between the predicted tellurium-oxygen coordination numbers and those measured using neutron diffraction.[44] The calculation suggests that tellurium should have, on average, ~0.5 more bonds to oxygen than measured. This mismatch was attributed to the overlap of the Te-O and O_B…O_B peaks in the correlation function. However, equation (8) is based upon the assumption that tellurium is entirely 4 coordinated in amorphous TeO_2 and that all oxygen atoms in the glass are bridging, bonding to two cations. Our recent neutron diffraction study of amorphous TeO_2 has indicated that approximately one in three tellurium atoms are three coordinated, yielding an average O-Te coordination number of 11/6.[13] This lower O-Te coordination number arises because each [TeO_3] unit must have one terminal oxygen (an oxygen double bonded to tellurium) associated with it to preserve stoichiometry. If the number of available oxygen atoms provided by each TeO_2 unit in the glass is corrected from 2 to 11/6, a new equation for the coordination number of tellurium with composition is calculated, given in equation (9)

$$n_{TeO}=\frac{2\left[3\mathrm{x}+\left(\frac{11}{6}\right)(100-x)\right]-2x*n_{BO}}{100-x} \qquad (9)$$

Using this revised equation, the differences between the calculated and measured values for n_{TeO} in the boron tellurite samples are reduced to ~0.2, as shown in Figure 9b. These values are closer to, but still significantly above, the measured values and the remaining discrepancy is attributed to the problem of deconvoluting the overlapping partials in the correlation function to extract the full Te-O bond distribution.

In contrast to the overlap between the Te-O and O_B…O_B peaks in the correlation functions for boron tellurites, there is much less difficulty in fitting the Te-O bond length distribution for aluminium

tellurite glasses as the Al-O peak which overlaps the Te-O peak can be simulated from ^{27}Al MAS NMR data (Figure 8). Therefore, equation (9) has been adapted to work for this system. Unfortunately, a direct adaptation, substituting n_{AlO} for n_{BO}, results in a change in n_{Teo} with composition that is too rapid. The mismatch between calculation and experiment cannot be accounted for by potential errors in extracting n_{TeO} from the neutron data as in this calculation nearly all the tellurium atoms would become ~3 coordinated by 12.5 mol% Al_2O_3. The Raman spectra for this glass composition in Figure S8c does not support this. An adjustment to the calculation was made to consider the possible effects on the presence of [AlO_6] units on the number of available oxygen bonds. In α-Al_2O_3 each oxygen atom forms four bonds to six coordinated Al atoms,[61] rather than two, to preserve electrostatic change balance. A revised version of equation 9 has been developed to take into account that Al-O bonds associated with [AlO_6] units need half the number of oxygen atoms that a [BO_n], [AlO_4] or [AlO_5] unit requires. This new equation to relate n_{AlO} and n_{TeO} is given in equation 10.

$$n_{TeO} = \frac{2\left[3x + \left(\frac{11}{6}\right)(100 - x)\right] - x * \frac{AlO_6}{Al} * 6 - 2x * \frac{AlO_5}{Al} * 5 - 2x * \frac{AlO_4}{Al} * 4}{100 - x} \quad (10)$$

The percentage of Al atoms in AlO_4, AlO_5 and AlO_6 units, measured using ^{27}Al MAS NMR, are given in Table 2 and were used in equation 10. The resultant calculated values for n_{TeO} are shown with those measured experimentally (taken from Table 5) in Figure 9b. There is excellent agreement between the two sets of values, with a difference of ≤ 0.03.

It should be noted that the suggestion of four coordinated oxygen associated with [AlO_6] units which has been made to explain the experimental results is unusual. However, the question of bonding in tellurites is complex.[62-63] Using bond valence there is an argument to be made that tellurium atoms in γ-TeO_2 are 5-coordinated and that these long bonds persist in the glass, playing a small but significant role in the network.[64] Long Te-O bonds in the tellurium-oxygen bond length distribution (r_{TeO} >1.97 Å) have a bond valence of less than one and so it is not unreasonable to consider that oxygen atoms in these bonds could accept several weak O-Al bonds to [AlO_6] units to help reach a total oxygen valence of 2. These longer Te-O bonds are primarily associated with [TeO_4] units ([TeO_3] units form three short bonds to oxygen with a bond valence of 1 or more) suggesting a possible link between [TeO_4] and [AlO_6] units in the glass. ^{17}O NMR experiments might provide useful insights on this.

In conclusion, an accurate value for the tellurium-oxygen coordination number can be calculated when the fractions of the [AlO_n] units in the glass are known. The monotonic decrease in the

coordination number of aluminium directly drives the decrease in the number of [TeO_3] units. Clearly with two phases present the model will best represent the dominant phase.

The equation derived above is an important step in improving the understanding of how tellurite glasses behave, showing that the same mechanism underpins the behaviour of tellurite glasses modified with two different trivalent cations, B_2O_3 and Al_2O_3. Extracting a tellurium-oxygen coordination number from neutron scattering data is difficult, requiring use of central facilities and multistage data analysis. The ability to predict the tellurium coordination number from ^{27}Al or ^{11}B NMR measurements is a significantly faster, cheaper and more accessible method for characterising the structure of the glass. However, to enable structure-property relationships to be developed for industrially relevant multicomponent glasses it is necessary to understand how a range of different network modifiers compete with each other for bonds to oxygen. A study of the interaction of Al_2O_3 and K_2O within a tellurite glass network is the logical next step as the individual behaviours of these two modifiers are now well understood.

4.4 Al…Al distances.

Each peak in a 2D double quantum spectrum corresponds to a particular combination of AlO_x units, thus the build–up of the [AlO_4-AlO_4] peak, which occurs at (54, 108) ppm, is not affected by AlO_6 or AlO_5. Similarly the [AlO_6-AlO_4] peak at (12, 66) ppm is not affected by nearby AlO_5 or AlO_6- Since the glass contains about 1/3 of each coordination this effectively reduces the already low concentration of Al to very low levels such that multispin effects are likely to be particularly small for the strongest interactions (shortest distances) such as AlO_4-AlO_4 and AlO_6-AlO_6. Note that a uniform dispersion of aluminium atoms throughout the 12.5 mol.% Al_2O_3 aluminium tellurite glass would give an average distance between any particular combination of aluminium atoms [AlO_n-AlO_m] of ~8 Å. For the higher Al content phase, assuming that the composition is ~ 8 mol.% richer, the closest [AlO_n-AlO_m] distance would still be > 7 Å. However, the existence of a relatively strong DQ signal shows that Al…Al distances are very much less than this. In particular there is a strong preference for like-like clustering of [AlO_4] and [AlO_6] in contrast to e.g. [AlO_5]-[AlO_5] units for which the signal is weak and the build-up slow, indicating that they are much further apart. It is not possible to make a precise estimate of the uncertainty in the distances but it can be seen from the simulations (figs 7 and S6) that a change in the dipole coupling corresponding to a distance change of 5% leads to a significantly worse agreement with experiment. Table 4 shows the distances, derived from the DQ build-up curves, between the [AlO_n] units which indicate that the [AlO_6] units are closest together, with a separation of ~3.2 Å, with [AlO_4] units being as close as 3.3 Å. In α-Al_2O_3, which is comprised solely of [AlO_6] units, there are two types of Al-O-Al distances present[61]: where two [AlO_6] units are edge sharing the distance between Al atoms is between 2.65-2.80 Å and where two [AlO_6] units are corner

sharing the distance between Al atoms increases to 3.20-3.50 Å. The distances found in this work therefore indicate that there is a fraction of corner sharing $[AlO_4]$-$[AlO_4]$ units and $[AlO_6]$-$[AlO_6]$ units in the glass but there are no direct (bonded through oxygen) linkages between other $[AlO_n]$ units. Unlike aluminium pairs have closest approaches of between 4.2 and 4.4 Å, while $[AlO_5]$ units are still further apart, > 4.7 Å. This corner sharing of $[AlO_4]$-$[AlO_4]$ units and $[AlO_6]$-$[AlO_6]$ units contrasts with the conclusion by Sakida *et al*.[27] that Al–O–Al bridging bonds are hardly formed in Al_2O_3–TeO_2 glasses in the composition range which they studied (≤14.3 mol% Al_2O_3). In high-alumina Al_2O_3-SiO_2 glasses formed by levitation melting Al…Al separations of 3.2 Å were observed by Weber *et al.*[51] using X-ray/ND difference functions. This preference for $[AlO_4]$-$[AlO_4]$ association and $[AlO_6]$-$[AlO_6]$ association is consistent with the derived relationship between aluminium and tellurium coordination numbers. As the concentration of Al_2O_3 in aluminium tellurites increases, there is an increase in the number of $[AlO_4]$ and $[TeO_3]$ units and a corresponding decrease in the fraction of $[AlO_6]$ and $[TeO_4]$ units. These changes suggest that some level of preferred bonding, and hence clustering, must occur. $[AlO_6]$ units are charge neutral if the oxygen atoms associated with them are four coordinated. In the above model, these Al_6-O bonds are the only ones assumed to have oxygens with such high coordination numbers, and so it is likely that $[AlO_6]$ units would cluster together to share oxygen atoms. The $[AlO_4]$ units which form as Al_2O_3 is added to the glass have an overall negative charge associated with them, which balances the formation of positively charged $[TeO_3]$ units. Therefore, it is also likely that $[TeO_3]^+$ and $[AlO_4]^-$ units cluster together. This tendency for clustering of $[AlO_6]$ units and of $[AlO_4]$ and $[TeO_3]$ units could be the source of the two T_g events in the aluminium tellurite glasses and, coupled with the effects of oxidation, provide the mechanism for the macroscopic crystal phase separation which is observed in the higher Al_2O_3 containing tellurite glasses.

5 Conclusions

This paper presents the first comprehensive structural study of aluminium tellurites where the tellurium-oxygen and aluminium-oxygen coordination numbers have been quantitatively determined using combined neutron scattering and ^{27}Al MAS NMR. Both the aluminium-oxygen and tellurium oxygen coordination numbers decrease as Al_2O_3 is added to the glass network. A reduction in the coordination number of tellurium with increased modifier content is consistent with an increase in the number of $[TeO_3]$ units present in the glass, in excellent agreement with the previously reported behaviour of tellurite glasses. However, unlike alkali tellurites, where the tellurium-oxygen coordination number does not change at low alkali oxide contents, the addition of Al_2O_3 reduces the tellurium-oxygen coordination number linearly. A direct linear correlation

between Te-O and Al-O environments is observed and a charge balance model has been successfully applied for the first time to predict the tellurium-oxygen coordination number using ^{27}Al MAS NMR alone. This model will best represent the dominant phase in the glasses. DQ MAS NMR measurements support these findings indicating that there is a significant fraction of corner sharing (~20%) for [AlO_4] units and [AlO_6] units. This occurs as [AlO_6] and [TeO_4] units dominate the network in TeO_2 rich glasses and $[AlO_4]^-$ units form to stabilise the presence of $[TeO_3]^+$ units as alumina is added to the glass. Clustering such as this could explain the presence of two T_g events in the aluminium tellurite glasses and indicate incipient phase separation in the glass that manifests when high concentrations of Al_2O_3 are present in the network.

6 Supporting Information

Figure S1: Density values for glasses used in this study compared with literature. **Figure S2:** Effect of pulse delay on ^{27}Al NMR MAS spectra obtained at 20 T from the 16 mol% Al_2O_3 aluminium tellurite sample. **Figure S3:** The low Q region (1-7 $Å^{-1}$) of the distinct scattering, $i(Q)$, for the 12.5 and 16 mol% Al_2O_3 samples showing Bragg peaks from α-Al_2O_3 and Al_2TeO_6. **Figure S4:** (a) A comparison of the NMR spectra collected at three different fields for the 10 mol% Al_2O_3 aluminium tellurite glass used to derive δ_{iso} and P_Q. **Figure S5:** Slices taken through the direct dimension in the DQ spectrum in Figure 6 of the main text in order to give an indication of the different distributions in intensity of the 4-6, 5-5, and 6-4 peaks. **Figure S6:** Experimental and simulated build up curves for the DQ MAS NMR experiment for all glass compositions. **Figure S7:** The isotropic shifts, δ_{iso}, reported for the different [AlO_n] species in Al_2O_3 glass and aluminate glasses plotted against the electronegativity values (Allred-Rochow) for Al and the second metal. **S8: Comments** on the microstructure of the glasses used in this study; **Figure S8a:** Typical SEM image of 12.5 mol% Al_2O_3 glass; **Figure S8b:** Typical SEM image of 10 mol% Al_2O_3 glass; **Figure S8c:** Micro-Raman spectra from 5 (blue), 10 (green) and 12.5 (red) mol% Al_2O_3 glasses; **Figure S8d:** Overlay of ^{125}Te static NMR spectra of 10 mol% Al_2O_3 (black) and 12.5 mol% Al_2O_3 (red) glasses (normalised to maximum intensity).

7 Acknowledgements:

Experiments at the ISIS Pulsed Neutron and Muon Source were supported by a beamtime allocation (RB 1210176) from Science and Technology Facilities Council. Special thanks are given to Professor Alex Hannon for support during the experiment. The UK 850 MHz solid-state NMR Facility used in this research was funded by EPSRC and BBSRC, as well as the University of Warwick including via part funding through Birmingham Science City Advanced Materials Projects 1 and 2 supported by

Advantage West Midlands (AWM) and the European Regional Development Fund (ERDF). We thank Steve York and Dr Ben Breeze for providing SEM/EDX and micro-Raman data respectively.

Tables

Nominal composition (mol% Al_2O_3)	Density +/- 0.01 (g/cm^3)	Density derived composition (mol% Al_2O_3)	XRF derived composition (mol% Al_2O_3)	Composition used in analysis (mol% Al_2O_3)	T_g1 (°C) ± 1	T_g2 (°C) ± 1
0	5.60	-	0	0	300	-
2.5	-	-	2.5	2.5		
5	5.373	5.35	5	5	329	364
10	5.125	10.53	9.89	10	354	396
15	5.037	12.37	12.40	12.5	361	405
20	4.889	15.47	16.24	16	380	419

Table 1: density, T_g and composition of the aluminium tellurite glasses.

Nominal composition (mol% Al_2O_3)	$[AlO_4]$ 55.5(5)*	$[AlO_5]$ 31.7(5)*	$[AlO_6]$ 5 (1)*	Avg. n_{AlO}	Avg. r_{AlO} (Å) ± 0.005
	% of each $[AlO_n]$ species present (±1)				
2.5	20	29	51	5.31(5)	1.867
5	24	30	46	5.22(5)	1.859
10	32	32	36	5.04(5)	1.845
12.5	35	33	32	4.97(5)	1.842
16**	37	28	35	4.98(5)	1.835

Table 2: Abundance of $[AlO_n]$ species present in the aluminium tellurite glasses and the resulting average aluminium-oxygen coordination number, n_{AlO}, which is used to calculate an average aluminium-oxygen bond length, r_{AlO}, using the relationship developed by Brese and O'Keefe. [57]
* Peak centroid (ppm) from integration. ** Average for samples not containing crystals.

species	δ_{iso} (ppm)	P_Q (MHz)	C_Q* (MHz)	W_q # (ppm)	W_{csd} (ppm)
$[AlO_4]$	55.7(5)	3.9(3)	3.7(1)	3.5(3)	8.4(6)
$[AlO_5]$	33(1)	3.1(3)	3.0(1)	7.5(7)	9.8(9)
$[AlO_6]$	8(1)	2.6(3)	2.5	5.3(4)	8.4(6)

Table 3: Chemical shifts, δ_{iso},, quadrupole parameters and contribution to the line width from chemical shift dispersion for the three Al co-ordination species in the 10 mol% Al_2O_3 aluminium tellurite glass.
*calculated assuming an η value of 0.5 (note maximal effect of η on Cq is 10%). # at 20 T (850 MHz).

	Al…Al distance (+/- 5%)		
Al unit	$[AlO_6]$	$[AlO_5]$	$[AlO_4]$
$[AlO_6]$	3.2	4.2	4.3
$[AlO_5]$	4.2	4.7	4.4
$[AlO_4]$	4.3	4.4	3.3

Table 4: The distances (+/- 5%) between different $[AlO_n]$ units in the 12.5 mol.%Al_2O_3 aluminium tellurite glass, derived from the DQ ^{27}Al MAS NMR build-up curves, that most closely match experiment assuming isolated spin pairs.

mol% Al_2O_3	$r_{TeO}A_{TeO}$	$2c_{Te}\bar{b}_{Te}\bar{b}_{O}$	n_{TeO}
0	0.83(1)	0.2244	3.69(5)
2.5	0.78(1)	0.2152	3.62(5)
5	0.74(1)	0.2063	3.58(5)
10	0.65(1)	0.1893	3.45(5)
12.5	0.62(1)	0.1812	3.41(5)
16	0.56(1)	0.1703	3.31(5)

Table 5: The integrated value for distance multiplied by area for the TeO peak in $T(r)$ and the derived tellurium–oxygen coordination numbers.

Figures

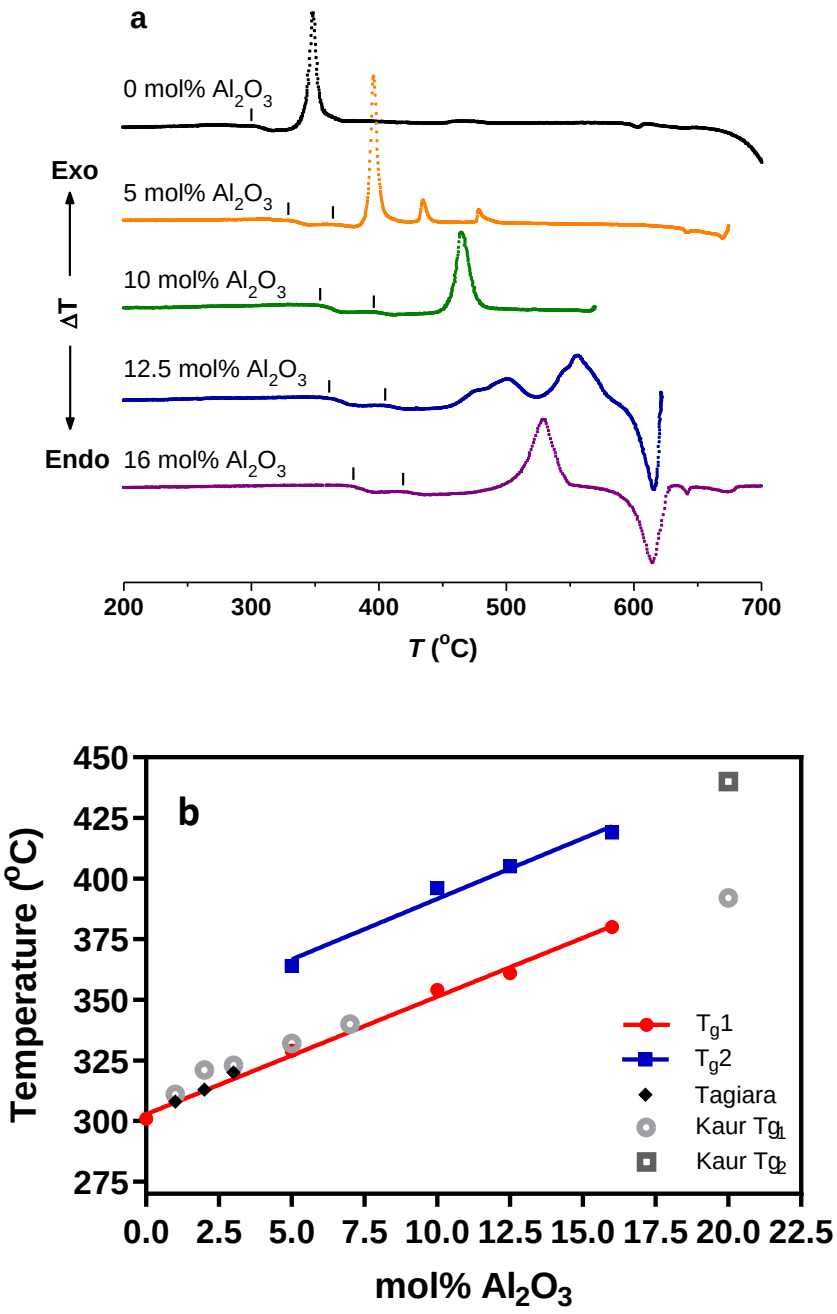

Figure 1: a) Differential Thermal Analysis scans for the aluminium tellurite glass samples and amorphous TeO_2.[13] The data are offset for clarity and tick marks indicate the glass transition events. b) the glass transition temperatures, T_g, plotted against composition for each sample. The T_g values reported by Tagiara et al. [26] and Kaur et al.[29] are also shown.

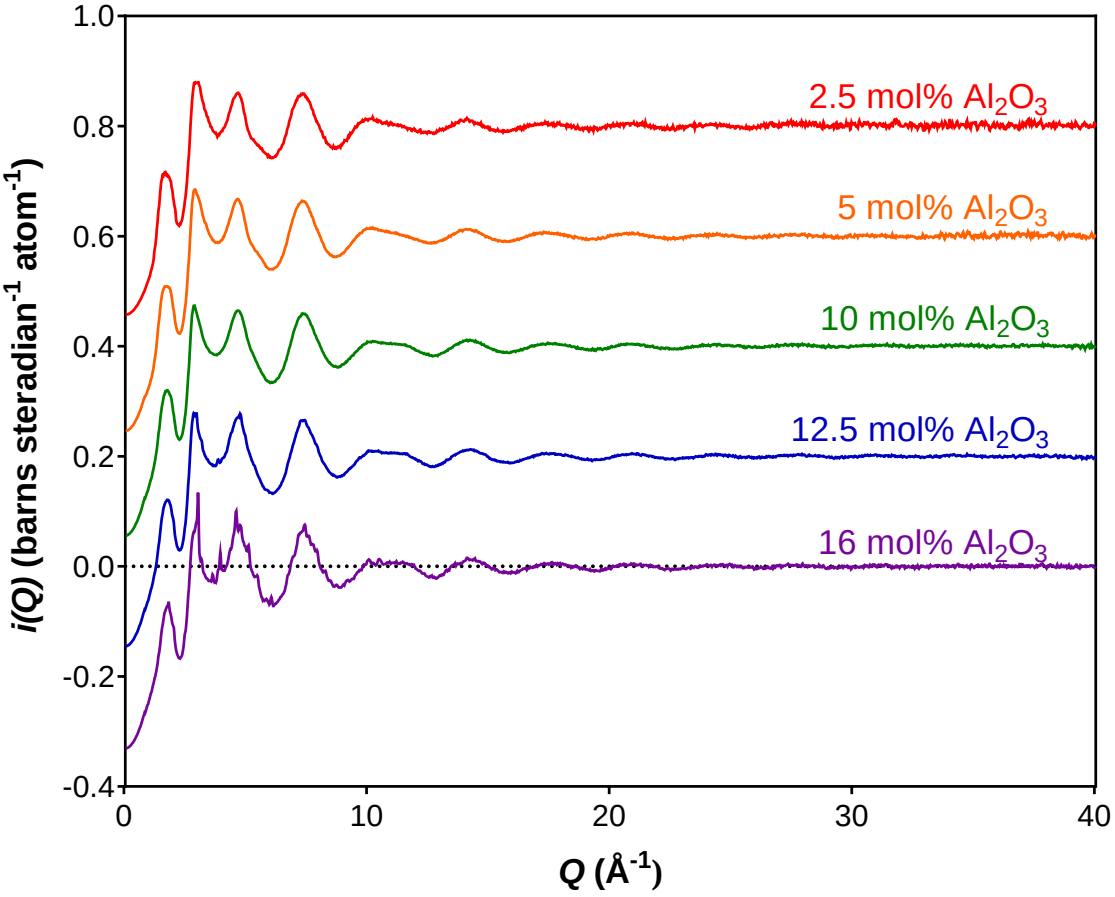

Figure 2: The distinct scattering, $i(Q)$, for the aluminium tellurite glass samples, with successive offsets of 0.2 for clarity.

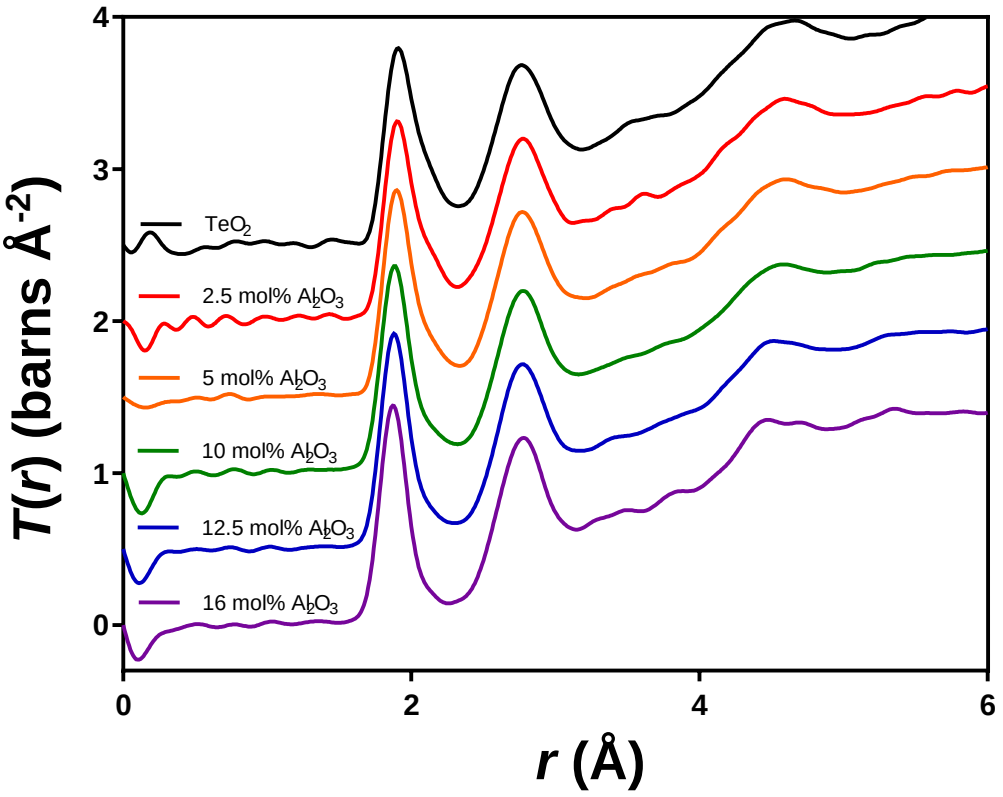

Figure 3: The total correlation functions, $T(r)$, for the aluminium tellurites shown with $T(r)$ for amorphous TeO_2.[13] Data are offset by 0.5 for clarity.

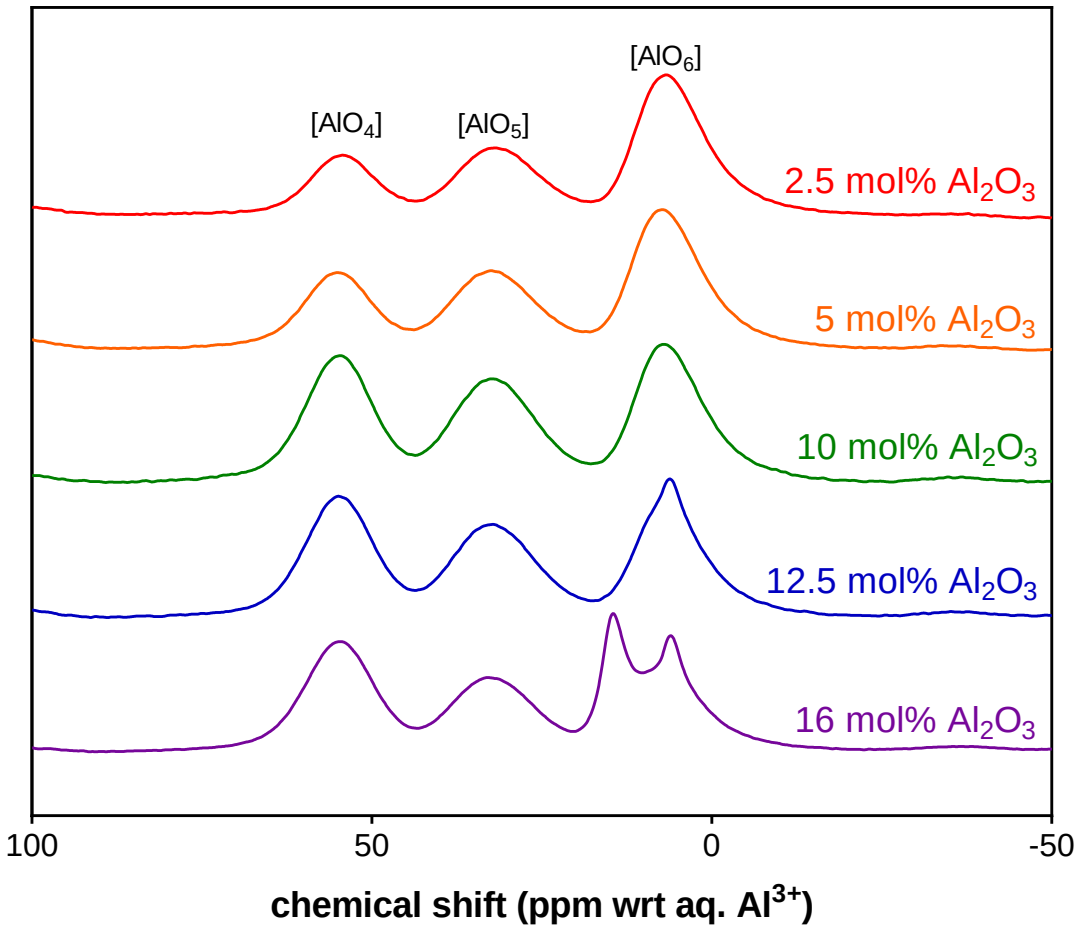

Figure 4: ^{27}Al MAS NMR spectra for all samples measured at 20 T. The peaks arising from [AlO_4], [AlO_5] and [AlO_6] species are readily identified. The data are offset for clarity.

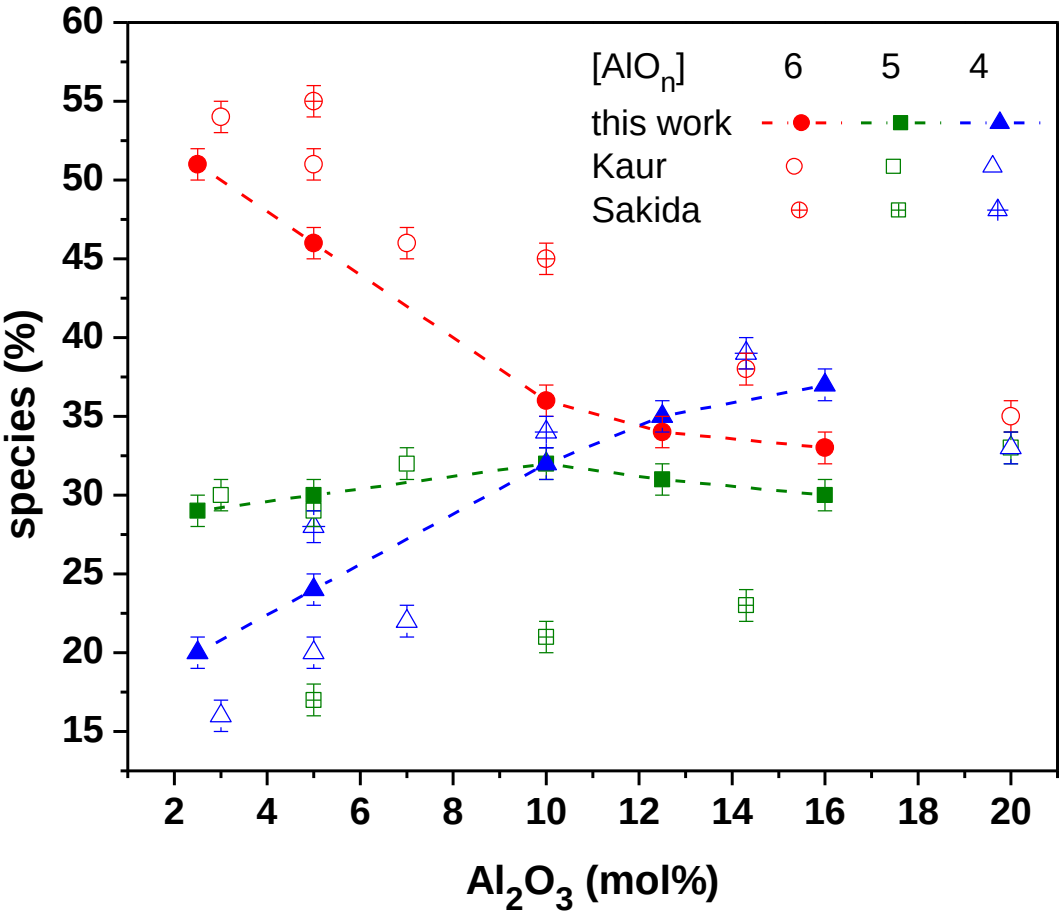

Figure 5: The percentages of [AlO_4], [AlO_5] and [AlO_6] units determined in each glass composition using ^{27}Al MAS NMR. The results from this study (solid shapes) are compared with those reported by Kaur *et al.* (open shapes)[29] and Sakida *et al*. (crossed shapes).[27]

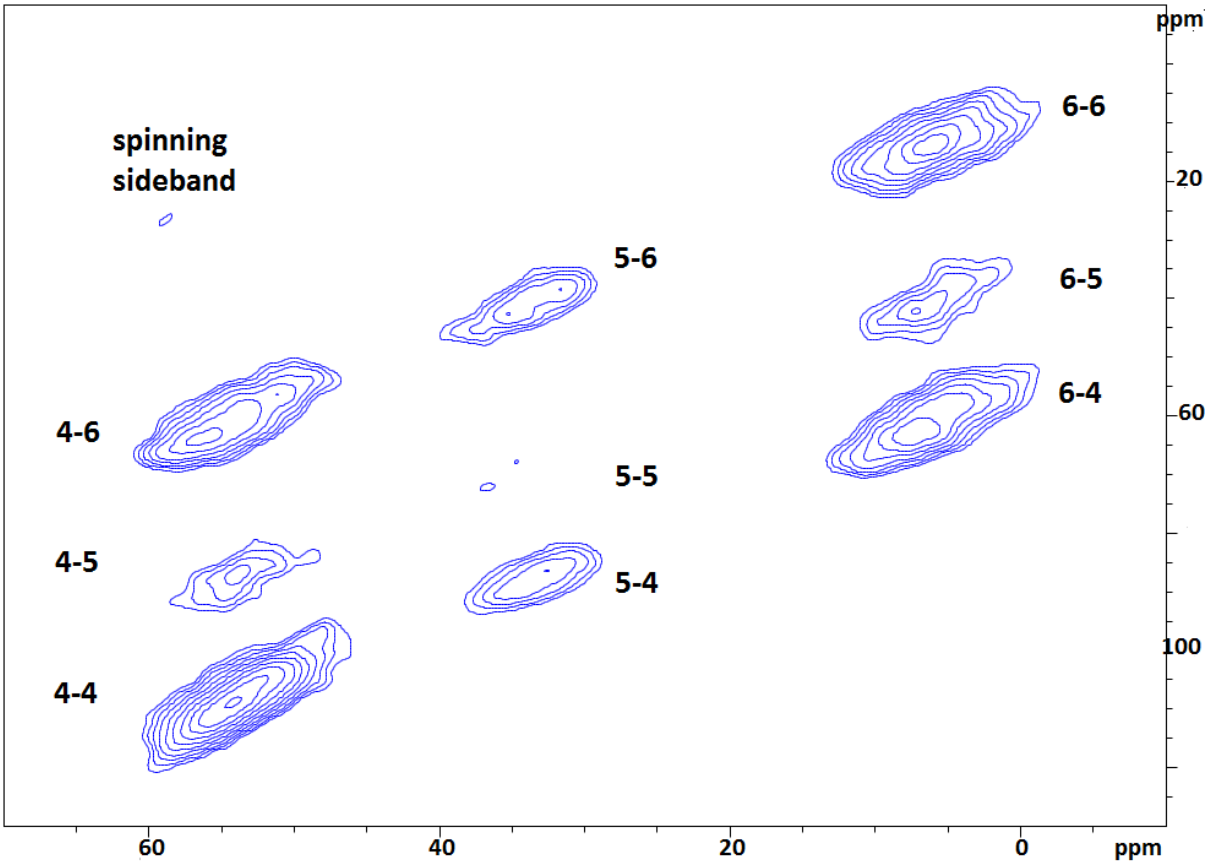

Figure 6: A 2D Double Quantum ^{27}Al MAS NMR spectrum for the 12.5 mol% Al_2O_3 aluminium tellurite glass collected with a mixing time of 3.2ms. Minimum contour 3.5%, multiplier 1.15

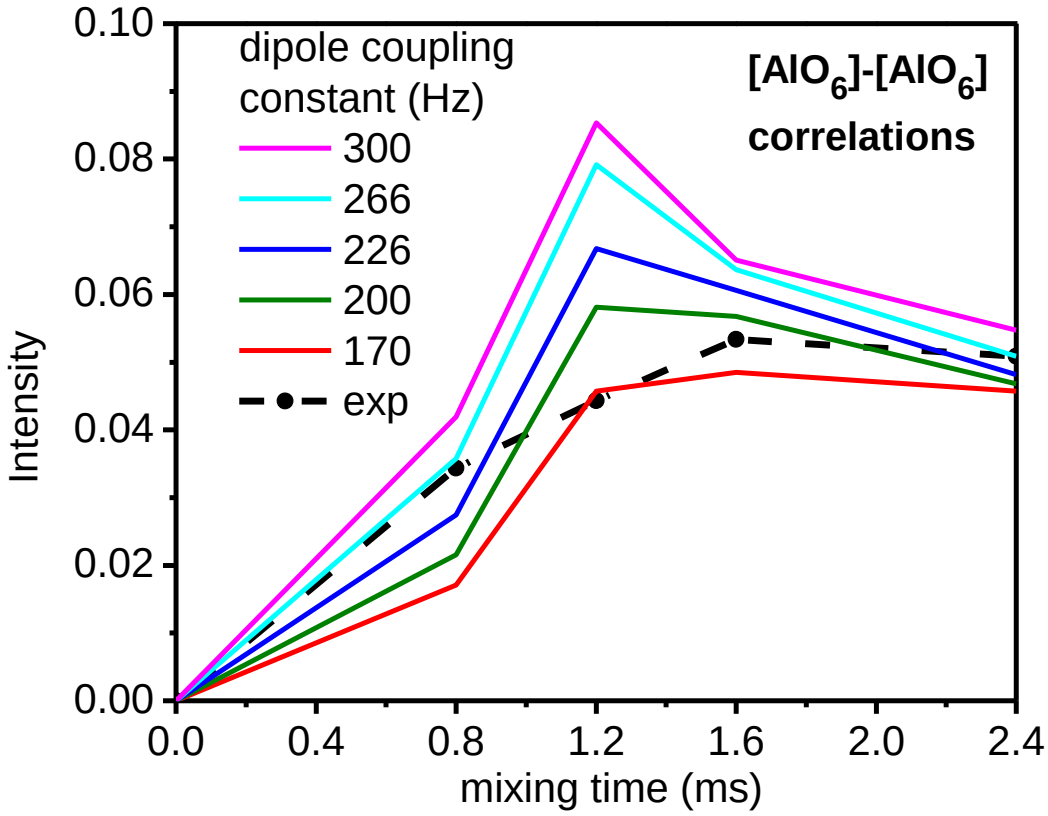

Figure 7: The experimental build-up curves for the [AlO_6] – [AlO_6] correlation at different mixing times together with the simulated intensities for a range of dipole coupling constants in Hz. Each simulated build up curve corresponds to a 5% change in distance. Build-up curves for other interactions are shown in the supplementary information.

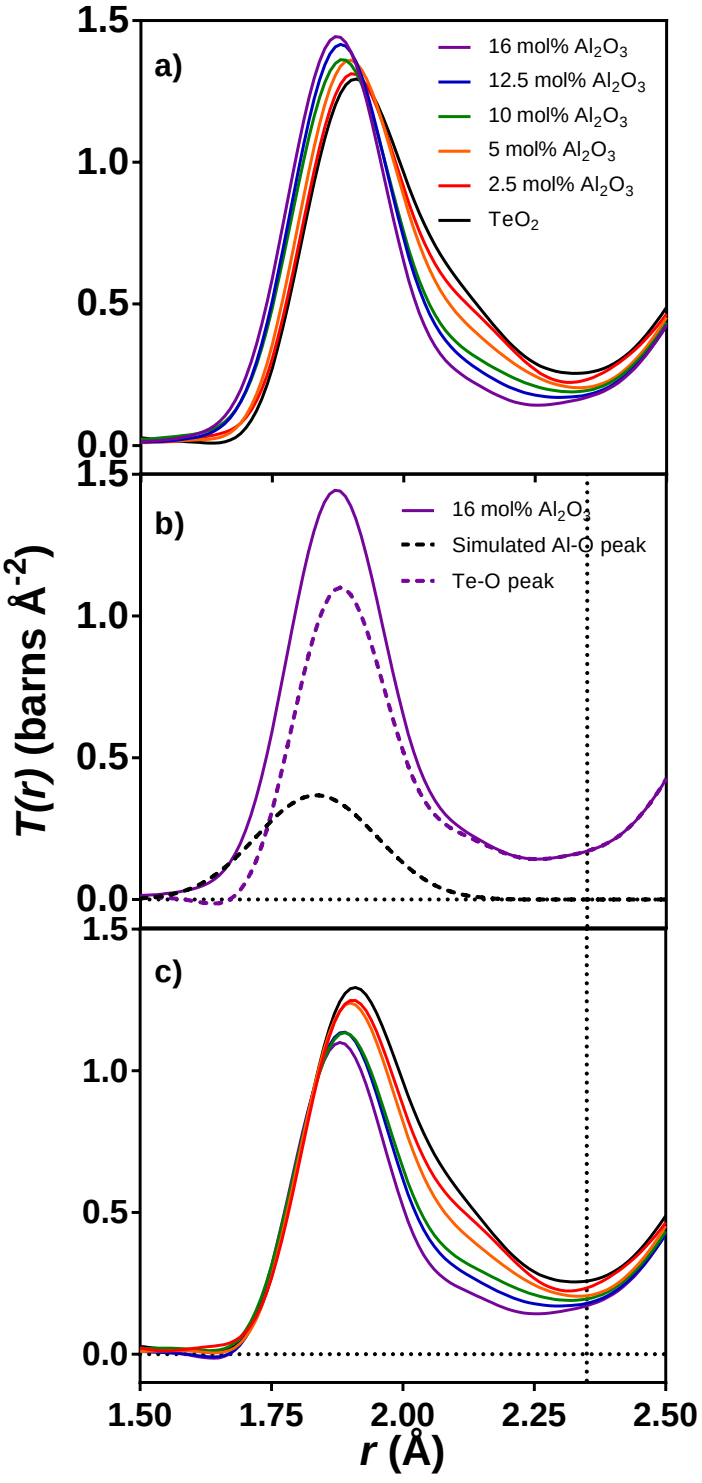

Figure 8: a) the first peak in the correlation function for the aluminium tellurites, b) the contribution to the first peak in the correlation function for the 16 mol% Al_2O_3 aluminium tellurite glass arising from Al-O bonds (black dashed line) and Te-O bonds (Purple dashed lines) and c) the first peak in the correlation function with the simulated contribution from Al-O bonds removed.

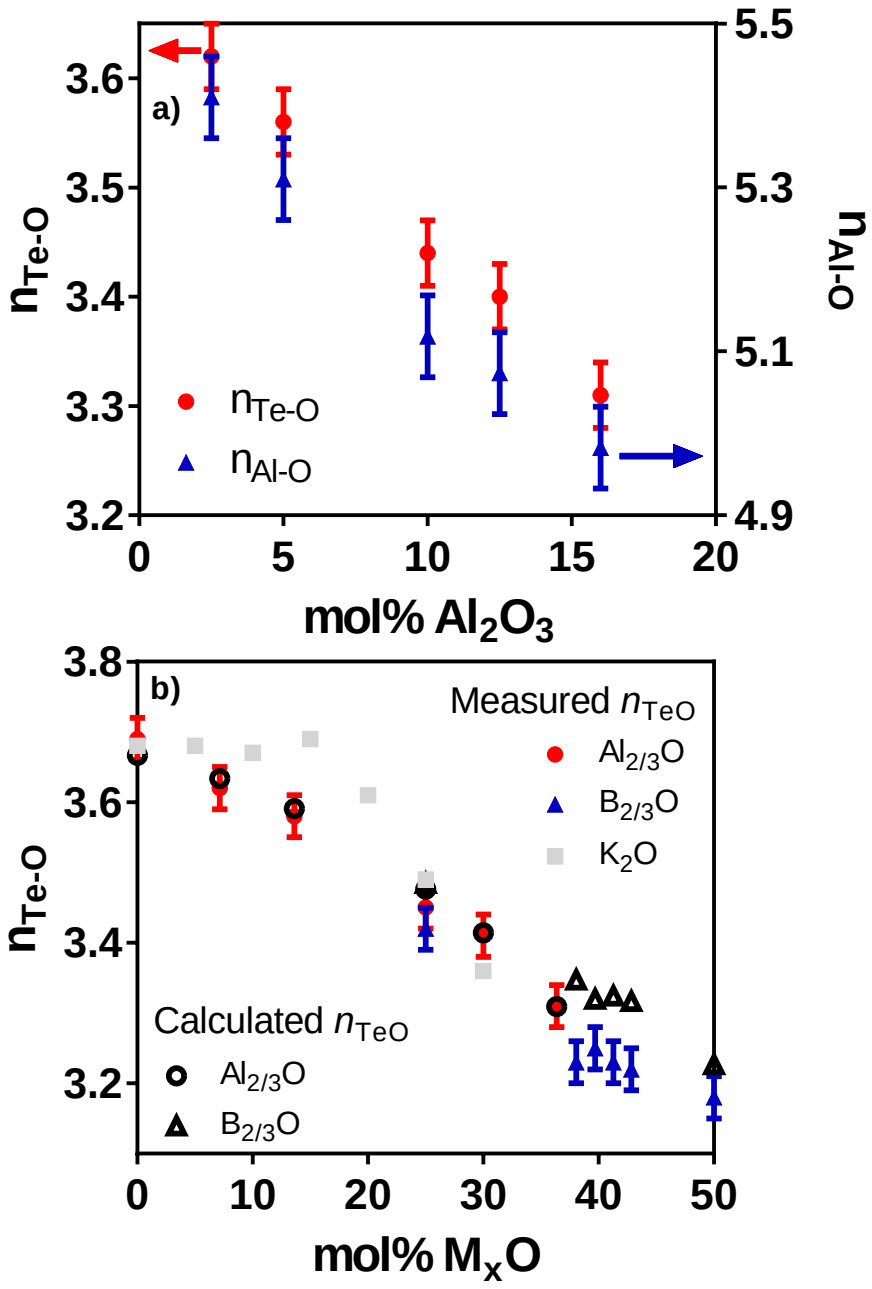

Figure 9: a) the change in tellurium-oxygen and aluminum-oxygen coordination numbers with aluminium oxide content and b) a comparison of the change in tellurium-oxygen coordination number with M_xO for potassium tellurites,[13] boron tellurites,[44] and aluminium tellurites (solid shapes). The open shapes show the calculated tellurium-oxygen coordination number for boron tellurites, using the boron-oxygen coordination number and equation 9,[44] and aluminium tellurites, using the aluminium-oxygen coordination number (Table 2) and equation 10.

8 References

1. Jha, A.; Richards, B. D. O.; Jose, G.; Fernandez, T. T.; Hill, C. J.; Lousteau, J.; Joshi, P., Review on Structural, Thermal, Optical and Spectroscopic Properties of Tellurium Oxide Based Glasses for Fibre Optic and Waveguide Applications. *Int. Mater. Rev.* **2012**, *57*, 357-382.
2. Berthereau, A.; Fargin, E.; Villesuzanne, A.; Olazcuaga, R.; LeFlem, G.; Ducasse, L., Determination of Local Geometries around Tellurium in TeO_2-Nb_2O_5 and TeO_2-Al_2O_3 Oxide Glasses by XANES and EXAFS: Investigation of Electronic Properties of Evidenced Oxygen Clusters by Ab Initio Calculations. *J. Solid. State Chem.* **1996**, *126*, 143-151.
3. Jha, A.; Richards, B.; Jose, G.; Teddy-Fernandez, T.; Joshi, P.; Jiang, X.; Lousteau, J., Rare-Earth Ion Doped TeO_2 and GeO_2 Glasses as Laser Materials. *Prog. Mater. Sci.* **2012**, *57*, 1426-1491.
4. Fargin, E.; Berthereau, A.; Cardinal, T.; LeFlem, G.; Ducasse, L.; Canioni, L.; Segonds, P.; Sarger, L.; Ducasse, A., Optical Non-Linearity in Oxide Glasses. *J. Non-Cryst. Solids* **1996**, *203*, 96-101.
5. El-Damrawi, G.; Hassan, A. K.; Doweidar, H., Silver Ionic Conductivity of Mixed Cationic Glasses. *Physica B Condens. Matter* **2000**, *291*, 34-40.
6. Prashant Kumar, M.; Sankarappa, T.; Vijaya Kumar, B.; Nagaraja, N., Dielectric Relaxation Studies in Transition Metal Ions Doped Tellurite Glasses. *Solid State Sci.* **2009**, *11*, 214-218.
7. Himei, Y.; Osaka, A.; Nanba, T.; Miura, Y., Coordination Change of Te Atoms in Binary Tellurite Glasses. *J. Non-Cryst. Solids* **1994**, *177*, 164-169.
8. McLaughlin, J. C.; Tagg, S. L.; Zwanziger, J. W., The Structure of Alkali Tellurite Glasses. *J. Phys. Chem. B* **2001**, *105*, 67-75.
9. Hoppe, U.; Yousef, E.; Russel, C.; Neuefeind, J.; Hannon, A. C., Structure of Vanadium Tellurite Glasses Studied by Neutron and X-ray Diffraction. *Solid State Commun.* **2002**, *123*, 273-278.
10. Kalampounias, A. G.; Nasikas, N. K.; Papatheodorou, G. N., Structural Investigations of the $xTeO_2$–$(1-x)GeO_2$ (x=0, 0.2, 0.4, 0.6, 0.8 and 1) Tellurite Glasses: A Composition Dependent Raman Spectroscopic Study. *J. Phys. Chem. Solids* **2011**, *72*, 1052-1056.
11. Tagg, S. L.; Huffman, J. C.; Zwanziger, J. W., Crystal Structure and Sodium Environments in Sodium Tetratellurite, $Na_2Te_4O_9$ and Sodium Tellurite Na_2TeO_3 by X-ray Crystallography and Sodium-23 NMR. *Chem. Mater.* **1994**, *6*, 1884-1889.
12. Barney, E. R.; Hannon, A. C.; Holland, D., Short-Range Order and Dynamics in Crystalline α-TeO_2. *J. Phys. Chem. C* **2012**, *116*, 3707-3718.
13. Barney, E. R.; Hannon, A. C.; Holland, D.; Umesaki, N.; Tatsumisago, M.; Orman, R. G.; Feller, S., Terminal Oxygens in Amorphous TeO_2. *J. Phys. Chem. Lett.* **2013**, *4*, 2312-2316.
14. Barney, E. R.; Hannon, A. C.; Holland, D.; Umesaki, N.; Tatsumisago, M., Alkali Environments in Tellurite Glasses. *J. Non-Cryst. Solids* **2015**, *414*, 33-41.
15. Zhang, M.; Boolchand, P., The Central Role of Broken Bond-Bending Constraints in Promoting Glass-Formation in the Oxides. *Science* **1994**, *266*, 1355-1357.
16. Zwanziger, J. W.; Tagg, S. L.; Huffman, J. C., Broken Bond-Bending Constraints and Glass Formation in the Oxides. *Science* **1995**, *268*, 1510.
17. Boolchand, P.; Zhang, M., Broken Bond-Bending Constraints and Glass-Formation in the Oxides - Reply. *Science* **1995**, *268*, 1510-1511.
18. Murugavel, S.; Roling, B., AC Conductivity Spectra of Alkali Tellurite Glasses: Composition-dependent Deviations from the Summerfield Scaling. *Phys. Rev. Lett.* **2002**, *89*, 195902.
19. Ghosh, A.; Bhattacharya, S., Comment on "AC Conductivity Spectra of Alkali Tellurite Glasses: Composition-dependent Deviations from the Summerfield Scaling". *Phys. Rev. Lett.* **2003**, *91*, 049601.
20. Murugavel, S.; Roling, B., Comment on "AC Conductivity Spectra of Alkali Tellurite Glasses: Composition-Dependent Deviations from the Summerfield Scaling" - Reply. *Phys. Rev. Lett.* **2003**, *91*, 049602.
21. Ghosh, A.; Pan, A., Scaling of the Conductivity Spectra in Ionic Glasses: Dependence on the Structure. *Phys. Rev. Lett.* **2000**, *84*, 2188-2190.

22. Kato, K.; Hayakawa, T.; Kasuya, Y.; Thomas, P., Influence of Al_2O_3 Incorporation on the Third-Order Nonlinear Optical Properties of Ag_2O-TeO_2 Glasses. *J. Non-Cryst. Solids* **2016**, *431*, 97-102.
23. Wang, P. F.; Wang, C. C.; Li, W. N.; Lu, M.; Peng, B., Effects of Al_2O_3 on the Thermal Stability, Glass Configuration of Yb^{3+}-doped TeO_2-K_2O-ZnO-Al_2O_3 Based Tellurite Laser Glasses. *J. Non-Cryst. Solids* **2013**, *359*, 5-8.
24. Nogami, M.; Abe, Y., Properties of Sol-gel-derived Al_2O_3-SiO_2 Glasses using Eu^{3+} Ion Fluorescence Spectra. *J. Non-Cryst. Solids* **1996**, *197*, 73-78.
25. Brovelli, S., et al., Efficient 1.53μm Erbium Light Emission in Heavily Er-doped Titania-modified Aluminium Tellurite Glasses. *J. Non-Cryst. Solids* **2007**, *353*, 2150-2156.
26. Tagiara, N. S.; Palles, D.; Simandiras, E. D.; Psycharis, V.; Kyritsis, A.; Kamitsos, E. I., Synthesis, Thermal and Structural Properties of Pure TeO_2 Glass and Zinc-Tellurite Glasses. *J. Non-Cryst. Solids* **2017**, *457*, 116-125.
27. Sakida, S.; Hayakawa, S.; Yoko, T., ^{125}Te, ^{27}Al, and ^{71}Ga NMR study of M_2O_3-TeO_2 (M = Al and Ga). *J. Am. Ceram. Soc.* **2001**, *84*, 836-842.
28. Youngman, R. E.; Aitken, B. G., NMR Studies of Aluminum Speciation in Tellurite Glasses. *J. Non-Cryst. Solids* **2001**, *284*, 9-15.
29. Kaur, A.; Khanna, A.; Gonzalez-Barriuso, M.; Gonzalez, F.; Chen, B. H., Short-range Structure and Thermal Properties of Alumino-Tellurite Glasses. *J. Non-Cryst. Solids* **2017**, *470*, 14-18.
30. Howells, W. S.; Hannon, A. C., LAD, 1982-1998: the First ISIS Diffractometer. *J. Phys.-Condes. Matter* **1999**, *11*, 9127-9138.
31. Soper, A. K. *GudrunN and GudrunX: Programs for Correcting Raw Neutron and X-ray Diffraction Data to Differential Scattering Cross Section*; RAL-TR-2011-013; Rutherford Appleton Laboratory: 2011.
32. Hannon, A. C.; Howells, W. S.; Soper, A. K., Atlas - a Suite of Programs for the Analysis of Time-of-Flight Neutron-Diffraction Data from Liquid and Amorphous Samples. *IOP Conf. Ser.* **1990**, *107*, 193-211.
33. Lorch, E., Neutron Diffraction by Germania, Silica and Radiation-damaged Silica Glasses. *J. Phys. C* **1969**, *2*, 229-237.
34. Lo, A. Y. H.; Eden, M., Efficient Symmetry-based Homonuclear Dipolar Recoupling of Quadrupolar Spins: Double-quantum NMR Correlations in Amorphous Solids. *Phys. Chem. Chem. Phys.* **2008**, *10*, 6635-6644.
35. States, D. J.; Haberkorn, R. A.; Ruben, D. J., A Two-Dimentional Nuclear Overhauser Experiment with Pure Absorption Phase in 4 Quadrants. *J. Magn. Reson.* **1982**, *48*, 286-292.
36. Bak, M.; Rasmussen, J. T.; Nielsen, N. C., SIMPSON: A General Simulation Program for Solid-state NMR Spectroscopy. *J. Magn. Reson.* **2000**, *147*, 296-330.
37. Wang, Q.; Hu, B.; Lafon, O.; Trebosc, J.; Deng, F.; Amoureux, J. P., Double-quantum Homonuclear NMR Correlation Spectroscopy of Quadrupolar Nuclei Subjected to Magic-angle Spinning and High Magnetic Field. *J. Magn. Reson.* **2009**, *200*, 251-260.
38. Mackenzie, K. J. D.; Smith, M. E., *Multinuclear Solid-state NMR of Inorganic Materials*, 1st ed.; Pergamon: Oxford, 2002; Vol. 6, p 702.
39. Dupree, R.; Farnan, I.; Forty, A. J.; Elmashri, S.; Bottyan, L., A MAS NMR-Study of the Structure of Amorphous Alumina Films. *J. Phys.* **1985**, *46*, 113-117.
40. Sato, R. K.; McMillan, P. F.; Dennison, P.; Dupree, R., A Structural Investigation of High Alumina Glasses in the CaO-Al_2O_3-SiO_2 System via Raman and Magic Angle Spinning Nuclear-Magnetic-Resonance Spectroscopy. *Phys. Chem. Glasses* **1991**, *32*, 149-156.
41. Dupree, R.; Lewis, M. H.; Smith, M. E., Structural Characterisation of Ceramic Phases With High-Resolution ^{27}Al NMR. *J. Appl. Crystallogr.* **1988**, *21*, 109-116.
42. Schmidt, B. C.; Riemer, T.; Kohn, S. C.; Behrens, H.; Dupree, R., Different Water Solubility Mechanisms in Hydrous Glasses Along the Qz-Ab Join: Evidence from NMR Spectroscopy. *Geochim. Cosmochim. Acta* **2000**, *64*, 2895-2896.

43. Ren, J. J.; Zhang, L.; Eckert, H., Medium-Range Order in Sol-Gel Prepared Al_2O_3-SiO_2 Glasses: New Results from Solid-State NMR. *J. Phys. Chem. C* **2014**, *118*, 4906-4917.
44. Barney, E. R.; Hannon, A. C.; Holland, D., A Multi-Technique Structural Study of the Tellurium Borate Glass System. *Phys. Chem. Glasses: Eur. J. Glass Sci. Technol. B* **2009**, *50*, 156-164.
45. Dimitriev, Y.; Kashchieva, E., Immiscibility in TeO_2-B_2O_3 System. *J. Mater. Sci.* **1975**, *10*, 1419-1424.
46. Burger, H.; Vogel, W.; Kozhukharov, V.; Marinov, M., Phase Equilibrium, Glass-forming, Properties and Structure of Glasses in the TeO_2-B_2O_3 System. *J. Mater. Sci.* **1984**, *19*, 403-412.
47. Su, X. M.; Wu, A. Y.; Vilarinho, P. M., Al_2TeO_6: Mechanism of Phase Formation and Dielectric Properties. *Scr. Mater.* **2012**, *67*, 927-930.
48. Sestak, V. Investigation of the system Al_2O_3-TeO_2-O_2. Masters Thesis, University of Missouri--Rolla, 1970.
49. Le Losq, C.; Neuville, D. R.; Florian, P.; Henderson, G. S.; Massiot, D., The Role of Al^{3+} on Rheology and Structural Changes in Sodium Silicate and Aluminosilicate Glasses and Melts. *Geochim. Cosmochim. Acta* **2014**, *126*, 495-517.
50. Neuville, D. R.; Cormier, L.; Montouillout, V.; Massiot, D., Local Al Site Distribution in Aluminosilicate Glasses by Al-27 MQMAS NMR. *J. Non-Cryst. Solids* **2007**, *353*, 180-184.
51. Weber, R.; Sen, S.; Youngman, R. E.; Hart, R. T.; Benmore, C. J., Structure of High Alumina Content Al_2O_3-SiO_2 Composition Glasses. *J. Phys. Chem. B* **2008**, *112*, 16726-16733.
52. Zhang, L.; Eckert, H., Sol–gel synthesis of Al_2O_3–P_2O_5 glasses: mechanistic studies by solution and solid state NMR. *J. Mater. Chem.* **2004**, *14*, 1605-1615.
53. Farnan, I.; Dupree, R.; Forty, A. J.; Jeong, Y. S.; Thompson, G. E.; Wood, G. C., Structural Information about Amorphous Anodic Alumina from Al-27 MAS NMR. *Philos. Mag. Lett.* **1989**, *59*, 189-195.
54. Lee, S. K.; Ryu, S., Probing of Triply Coordinated Oxygen in Amorphous Al_2O_3. *J. Phys. Chem. Lett.* **2018**, *9*, 150-156.
55. Thomsen, R. M.; Skibsted, J.; Yue, Y., The Charge-Balancing Role of Calcium and Alkali Ions in Per-Alkaline Aluminosilicate Glasses. *J. Phys. Chem. B* **2018**, *122*, 3184-3195.
56. Hannon, A. C.; Barney, E. R.; Holland, D., The Structure of Tin Borate Based Glasses. *Phys. Chem. Glasses* **2009**, *50*, 271-283.
57. Brese, N. E.; O'Keeffe, M., Bond-Valence Parameters for Solids. *Acta Cryst. B* **1991**, *47*, 192-197.
58. Becker, C. R.; Tagg, S. L.; Huffman, J. C.; Zwanziger, J. W., Crystal Structures of Potassium Tetratellurite, $K_2Te_4O_9$, and Potasium Ditellurite, $K_2Te_2O_5$, and Structural trends in Solid Alkali Tellurites. *Inorg. Chem.* **1997**, *36*, 5559-5564.
59. Sekiya, T.; Mochida, N.; Ohtsuka, A.; Soejima, A., Raman Spectra of $BO_{2/3}$-TeO_2 glasses. *J. Non-Cryst. Solids* **1992**, *151*, 222-228.
60. Sekiya, T.; Mochida, N.; Ohtsuka, A.; Soejima, A.; Yasumori, A.; Yamane, M., 11B MAS NMR spectra of $BO_{3/2}$-TeO_2 glasses. *Glastech. Ber.* **1993**, *66*, 15-20.
61. Finger, L. W.; Hazen, R. M., Crystal-Structure and Compression of Ruby to 46 Kbar. *J. Appl. Phys.* **1978**, *49*, 5823-5826.
62. Alderman, O. L. G.; Benmore, C. J.; Feller, S.; Kamitsos, E. I.; Simandiras, E. D.; Liakos, D. G.; Jesuit, M.; Boyd, M.; Packard, M.; Weber, R., Short-Range Disorder in TeO2 Melt and Glass. *J. Phys. Chem. Lett.* **2020**, *11*, 427-431.
63. Garaga, M. N.; Werner-Zwanziger, U.; Zwanziger, J. W.; DeCeanne, A.; Hauke, B.; Bozer, K.; Feller, S., Short-Range Structure of TeO_2 Glass. *J. Phys. Chem. C* **2017**, *121*, 28117-28124.
64. Champarnaud-Mesjard, J. C.; Blanchandin, S.; Thomas, P.; Mirgorodsky, A.; Merla-Mejean, T.; Frit, B., Crystal Structure, Raman spectrum and Lattice dynamics of a new metastable form of tellurium dioxide: γ-TeO_2. *J. Phys. Chem. Solids* **2000**, *61*, 1499-1507.

9 TOC Image

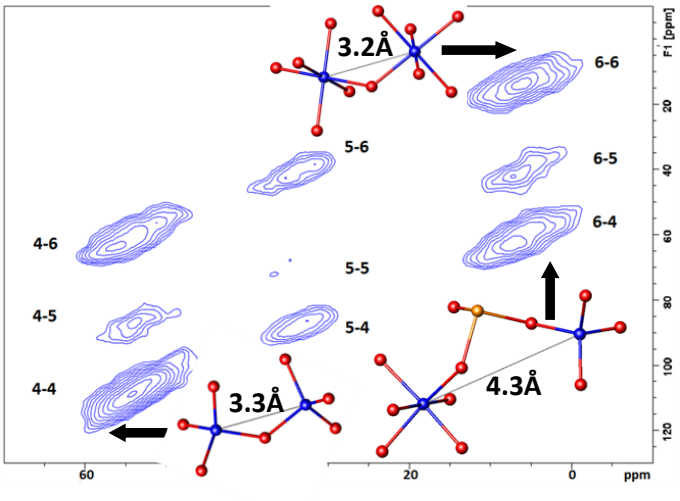
3.2Å
6-6
5-6
6-5
6-4
4-6
5-5
4-5
5-4
4-4
3.3Å
4.3Å
F1 [ppm]
20
40
60
80
100
120
60
20
0
ppm